

Energy-Latency Optimization for Dynamic 5G Mobile Radio Access Networks

Gabriela N. Caspa H., *Student Member, IEEE*, Carlos A. Astudillo, *Member, IEEE*, and Nelson L. S. da Fonseca, *Senior Member, IEEE*

Abstract—In 5G networks, base station (BS) disaggregation and new services present challenges in radio access network (RAN) configuration, particularly in meeting their bandwidth and latency constraints. The BS disaggregation is enabled by functional splitting (FS), which distributes the RAN functions in processing nodes and alleviates latency and bandwidth requirements in the fronthaul (FH). Besides network performance, energy consumption is a critical concern for mobile network operators (MNO), since RAN operation constitutes a major portion of their operational expenses (OPEX). RAN configuration optimization is essential to balance service performance with cost-effective energy consumption. In this paper, we propose a mixed-integer linear programming (MILP) model formulated with three objective functions: (i) minimizing fronthaul (FH) latency, (ii) minimizing energy consumption, and (iii) a bi-objective optimization that jointly balances both latency and energy consumption. The model determines the optimal FS option, RAN function placement, and routing for eMBB, URLLC, and mMTC slices. Although prior studies have addressed RAN configuration either from an energy minimization or latency reduction perspective, few have considered both aspects in realistic scenarios. Our evaluation spans different topologies, accounts for variations in aggregated gNB demand, explores diverse FS combinations, and incorporates Time Sensitive Networking (TSN) modeling for latency analysis, as it is also crucial in RAN performance. Given that MILP’s execution time can be significant, we propose a heuristic algorithm that adheres to RAN constraints. Our results reveal a trade-off between latency and energy consumption, highlighting the need for dynamic RAN reconfiguration. These insights provide a foundation to optimize existing and future RAN deployments.

Index Terms—RAN, functional split, time sensitive networks, latency, energy, optimization.

I. INTRODUCTION

THE fifth generation (5G) of mobile networks evolves the RAN to attend the growing demand of mobile applications and to support three types of services namely enhanced mobile broadband (eMBB), ultra-reliable low latency communications (URLLC), and massive machine-type communications (mMTC). Each of them has unique characteristics and requirements; for instance, eMBB demands high bandwidth in use cases as multimedia services or augmented reality. URLLC requires low latency and high reliability, some use cases involve vehicular communications or e-health. mMTC needs to support a high number of connections such as Internet of Things (IoT) deployments. On the other side, base stations

This work was supported by the São Paulo Research Foundation (FAPESP) under grant number 2023/00673-7, and by the Brazilian Federal Agency for Support and Evaluation of Graduate Education (CAPES) 88882.329100/2014-0.

Gabriela N. Caspa, C. A. Astudillo and N. L. S. da Fonseca are with the Institute of Computing, University of Campinas 13083-852, Brazil. (e-mails: gabriela@lrc.ic.unicamp.br, castudillo@unicamp.br, nfonseca@ic.unicamp.br).

are disaggregated with functional splitting (FS) to reduce RAN OPEX and CAPEX while alleviating stringent RAN requirements of bandwidth and latency. Initially, C-RAN intended to reduce capital expenditure (CAPEX) and to enhance cell coordination among gNBs by centralizing baseband functions in a processing pool (PP). This approach connected the Radio Frequency (RF) module to the PPs via a network known as mobile FH. However, that arrangement led to a high bandwidth utilization in the FH even with low demand, owing to the constant bit rate (CBR) produced by separating the RF and low-physical functions. Additionally, C-RAN FH latency is constrained to 250 μ s due to the time restriction imposed by Hybrid Automatic Repeat Request (HARQ) mechanism messaging.

To overcome the C-RAN strict requirements, FS is introduced to split the gNB into three entities: radio unit (RU), distributed unit (DU), and centralized unit (CU); where the FH connects the RU to the DU, and the midhaul (MH) interconnects the DU and the CU. Thanks to the advances on virtualization, the RAN protocol stack of gNB is virtualized and can be deployed as virtualized network function (VNF) into commercial-off-the-shelf (COTS) hardware. These functions reside in the DU and CU, which can be placed on centralized or edge PPs. The RU, placed in the cell-site, handles the RF portion with specialized hardware. Hence, the RAN functions are distributed among the RU, DU, and CU according to a FS option that describes where the function chain should be placed among those units. The 3GPP considers eight FS options, and the C-RAN approach is equivalent to the FS option 8. The rest of FS options allows RAN flexibility and relieves the FH bandwidth and latency restrictions because: a) it offers alternatives to the CBR of C-RAN by letting FH/MH load vary according to actual gNB demand, b) the RAN functions can be placed in different PPs locations, and c) a PP can hold virtualized functions of more than one gNB. This flexibility enables slice design to balance latency and bandwidth by adapting function placement to service needs.

As latency requirements are critical in RAN, the transport network needs to apply advanced technologies to ensure deterministic performance while maintaining cost efficiency. In this line, packet-switched networks were proposed in the disaggregated RAN transport network using Ethernet frame encapsulation [1]. This approach led to the convergence of FH and MH, referred to as crosshaul (XH), creating a unified transport layer. Within this context, TSN is proposed as a suitable solution for packet-based RAN to meet strict latency requirements [2]. It enables deterministic, low-latency communication in the XH by prioritizing frames according to latency classes. In addition, a packet-based XH can decrease deployment costs by avoiding dedicated point-to-point fiber links and to take advantage of

legacy Ethernet infrastructure [3].

RAN energy consumption accounts for almost 75% of mobile networks and nearly 40% of RAN OPEX, emphasizing the need for more efficient use of RAN network and computing resources [4]. RAN disaggregation offer the flexibility to dynamically reconfigure the network to match service demand. However, this flexibility introduces new challenges: the RAN configuration problem is NP-hard, involving interdependent decisions on functional split (FS) selection, virtual network function (VNF) placement, and transport (XH) routing. Each FS option imposes different latency and bandwidth requirements on the FH and MH, while routing decisions impact delay and energy usage, due to the need of activation of network and processing resources. This creates an inherent trade-off between minimizing latency and reducing energy usage in dynamic RAN environments.

Prior studies have addressed the RAN configuration problem from various perspectives, often focusing on cost reduction, spectrum efficiency, or service admission control to improve MNO profitability. However, energy consumption and latency are frequently treated in isolation or oversimplified, although these are critical factors in the RAN configuration. While some works aim to reduce OPEX with FS selection or VNF placement, few works explicitly address the energy consumption of both PPs and transport elements. Also, latency is often simplified using fixed or average values, disregarding queuing delays that influence FS decisions. Some research works employ optimal approaches using MILP, yet these proposals require high execution time and are assessed on small-scale scenarios. To overcome those limitations, heuristics or artificial intelligence were proposed with approximate results.

In this work, we focus on RAN configurations to achieve lower energy consumption while satisfying the requirements of heterogeneous use cases on a sliced-based scenario. We specially study the FS selection effects on the energy consumption, FH latency, and resource utilization in a packet-switched RAN. Our contributions include:

- We propose a MILP model to address the RAN configuration problem from an energy and latency perspective. The model performs FS selection, function placement, and routing constrained to network and computing resources. The model includes a deterministic latency estimation and energy consumption of PPs and network equipment. The executing time is not significant in medium-size topologies, but it increases with the number of edges.
- An heuristic is proposed to tackle the previous problem with less executing time and complexity, so it can be applied to larger scenarios.
- We evaluate both algorithms in different realistic scenarios, many FS combinations denominated virtual configuration (VC), and consider varying gNB traffic demand throughout a day. We study the tradeoff between energy minimization, FH latency prioritization and a midpoint between them. In addition, we observe the VC selection variance among use cases and its influence on resource utilization.

The rest of this article is organized as follows. In Section II, we present the related work. Section III describes the system model, discusses characteristics of combinations of FS as

virtual configurations, and presents the computing and latency model employed in the MILP. In Sections IV and V the MILP and heuristic are detailed, respectively. Then Section VI the experimental results are exhibited. Finally, we conclude the article in Section VII

II. RELATED WORKS

The literature on RAN configuration has explored various aspects including OPEX minimization, service admission control, spectrum utilization, energy consumption, and latency. In this section, we review and classify related works based on the main concerns of this proposal: FS selection, slice resource optimization, and RAN energy and latency. A summary of these works is presented in Table Table I including the main aspects studied in this article.

A. Selection of Functional Splitting

In [5], Alba *et al.* presents one of the earliest works of FS adaptation at runtime. They highlight the need, objectives, and challenges of dynamic FS selection, emphasizing the limitations of static configurations. The authors implement an adaptive RAN that changes the split over time and evaluate its impact on packet loss and delay. However, the study is limited to only two FS options in a simplified architecture, and does not address RAN slicing. Next, focusing on the viability and profitability of the split adaptation, the authors of [6] propose a MILP to select the optimal FS of a given RAN network. They also introduce a cost-of-flexibility framework to assess FS adaptation overhead and propose strategies to decide when reconfiguration is needed. However, they do not consider network slicing, service-specific requirements, or RAN energy consumption.

The authors of [7] and [8] tackled the joint problem of FS selection, RAN placement and path selection with a Binary Integer Linear Programming (BILP) and deep reinforcement learning approaches. In both works, they aim at reducing RAN computing utilization and maximize the RAN centralization level. Their proposed architecture considers both single and dual split options for RAN function placement. The deep reinforcement learning work was elaborated to reduce the solving time compared to the optimal approach. Conversely, Amiri *et.al.*, in [9], employ FS selection to balance the computing load of CUs and transmission load in the FH network over an O-RAN architecture to minimize the operation costs. They first model the scenario resulting in a NP-hard problem, thus they resolve it with an heuristic algorithm. Even though the problem considers dynamic FS, energy and latency are not studied in detail.

B. RAN Slicing

The authors in [10] and [11] enable RAN slicing with two frameworks using SDN and virtualization. First, FlexRAN enables real-time control via a hierarchical architecture. Orion performs RAN slicing through a hypervisor that virtualizes radio, computing, and spectrum resources. However, these works do not address function split selection nor consider latency or energy consumption.

In [12], the authors propose a resilient slice embedding strategy for uRLLC services based on Dedicated Path Protection

(DPP) and functional splitting. Their heuristic minimizes physical resource allocation while ensuring reliability against node or link failures. The algorithm considers various FSs and performs function chaining under distance and processing constraints. However, it focuses exclusively on URLLC slices and does not address energy or latency optimization.

Ojaghi has worked on FS and slicing in the works [13], [14], [15], and [16]. These works tackled different RAN problems with MILP and most of them included an heuristic. The first two seek to maximize the network throughput while satisfying heterogeneous slice requirements. The approaches included a customized FS per slice, unit placement and routing while satisfying Service Legal Agreement (SLA) per service. Then, in [15], MEC placement is included in the problem to provide edge services. Finally, in [16], an heuristic is proposed to analyze the performance of joint slicing and FS in dense networks. However, the RAN architecture is simplified assuming the DU and RU are co-allocated, and RAN energy consumption is overlooked.

In [17], the authors propose a MILP-based framework that considers slice design for different types of services and dynamic FS. They focus on the impact of slice isolation levels in the physical network and map new isolation and SLA constraints that influence in the FS decision. They seek to minimize the number of active nodes, links and reconfigurations by evaluating different FS and slice sharing policies. Although slicing, and dynamic FS are addressed in the article, the work disregards latency and energy.

Sen et al. elaborated a MILP in [18] that maximizes the RAN centralization degree to reduce the number of processing nodes. They also propose an heuristic as an alternative with lower computing complexity. Their approach selects a specific FS and performs unit placement per slice. The slices serve 5G services like eMBB, URLLC, and mMTC, but specific latency and bandwidth requirements are not specified. Also RU configurations (channel bandwidth, modulation, number of layers) remain as in 4G. Besides, latency analysis is simplified with fixed values for the FH and MH delay.

In [19], the authors address the slice-admission control problem to maximize the RAN long-term revenue. Their work involves multi-agent deep reinforcement learning that accepts or decline slice requests based on computing, bandwidth, and transmission resource availability, considering service-specific requirements. Each slice is assigned a FS option among the standardized FS options 2, 6, and 7. Their work is compared with two heuristics: greedy and node-ranking, and a single-agent approach. However, this work focuses on the resource utilization and simplifies the latency analysis.

C. Energy and Latency in RANs

In [20], the authors address the joint optimization of FS selection, BBU server allocation, and scheduling in a C-RAN architecture to minimize end-to-end latency. The model uses an M/D/1 queue to represent BBU processing with deterministic job sizes dependent on the FS, and includes delay contributions from BBU processing, FH transport, and RRH computation. Two objectives are studied: minimizing the total average delay and the maximum average delay across streams. While the

approach allows flexible FS and detailed delay modeling, it does not incorporate slicing or energy-related aspects.

In [21], the authors apply reinforcement learning to minimize RAN OPEX by dynamically selecting both the functional split and energy source. The approach reduces CU and DU energy consumption by leveraging renewable energy and adapting the FS to daily traffic variations. It consider eMBB and URLLC slices requirements, assigning a FS to each. However, latency is not analyzed, and the model assumes that DU and RU are always co-located at the same site and the gNB placement is already given.

In [22], the authors propose a constrained deep reinforcement learning model to minimize DU and CU energy consumption through dynamic FS adaptation per RU in a virtualized RAN. However, slicing is not explicitly addressed and latency is not studied in detail. As a continuation of this previous work, in [23] the authors develop a framework that allows dynamic vRAN reconfiguration on-the-fly. They work on an O-RAN architecture and focus on reconfiguring several aspects of the RAN: functional split selection, resource allocation, unit placement, gNB association, and routing. The goal is to minimize the long-term total network cost. Yet, these works do not consider slicing requirements nor dive into latency details.

Klinkowski applied MILP in the RAN planning problem considering both latency and computing in their works [24] and [25]. In their first work, he focuses on the CU and DU placement problem, and simplifies the routing with a single candidate path. In the second work, the author proposes a MILP and a simulated annealing algorithm that jointly minimizes the number of active processing nodes and FH latency. The algorithms performs CU, DU, and RU placement, and path selection. The configuration per RU can set single or double split employing FS options 7 or 2. An analysis for the delays is performed following time-sensitive-networks queuing algorithm. Nonetheless, this work does not consider slicing requirements for 5G use cases nor energy consumption.

In the work [26], the authors propose a MILP and heuristic algorithm to minimize the RAN power consumption. These algorithms choose a FS option between options 2 or 7, perform unit placement and path selection. The MILP has high computational demands even for medium topologies, while the heuristic achieves near-optimal results with significantly lower solving time. They consider PP power consumption, but ignore network power consumption. Also, a brief latency analysis is included from the work [24]; however, latency is not explored. Slices are considered but the 5G use cases restrictions are not included.

In [27], the authors propose a two-step approach to minimize both CAPEX and OPEX. The cost model includes backhaul connectivity, fronthaul deployment, energy consumption of processing nodes, network maintenance, and BBU pool rental. They first propose a recursive algorithm to get candidate processing pools and optic aggregators, then, a MILP provides optimal unit placement and routing. They also analyze the G/G/1 model for queuing delay in RAN. However, a fixed FS is considered (option 7) and network equipment energy, and slicing are overlooked.

The work in [28] presents a MILP that jointly minimizes

TABLE I: Literature review

Article	Approach	Objective	Latency	Energy	5G	DFS	Slicing
[29]	MILP, Heuristic	Min. PP power consumption	Static, queuing delay	PP, DC	No info	Yes	No
[24], [25]	MILP, Heuristic	Min. active PP & FH latency	Static, queuing delay	No	8 MIMO, 32 antenna, 100 MHz	No	No
[15], [14], [16]	MILP, Benders decomposition algorithm	Max. throughput & Min. slice cost	Processing, transmission, propagation	No	100 PRBs, 20 MHz, 2x2 MIMO, 28 MCS	Yes	Yes
[27]	MILP, Recursive clustering algorithm	Min. energy consumption and maintenance cost	Queuing G/G/1	PP, RU	10, 20, 40, and 100 MHz	No	No
[6], [5]	MILP	Min. OPEX & Max. spectral efficiency	Propagation, processing	No	No info	Yes	No
[23], [22]	DRL	Min. OPEX (routing and computing)	Fixed values	No	SISO, 10 MHz LTE, 36.6 Mbps	Yes	Yes
[28]	MILP, Heuristic	Min. power consumption & handover	No	CU	No info	No	No
[30]	DRL	Min. OPEX: routing, computing	Static	No	100 MHz spectrum, 4x4 MIMO, 16QAM	Yes	No
[8]	DRL	Min. computing usage, Max. centralization	Fixed values	No	No info	Yes	No
[19]	DRL	Max. long-term revenue	Fixed values	No	20 MHz, 2x2 MIMO, 64QAM	No	Yes
[31]	MILP, e-constraint, Pareto	Min. energy consumption - Max. RAN centralization	Fixed values	PP	No info	No	No
[21]	RL	Min. energy consumption	No	PP	No info	Yes	Yes
[17]	MILP	Min. CAPEX (slice creation cost)	Fixed values	No	No info	Yes	Yes
[32]	MILP, Heuristic	Min. 2E2 Latency	Queuing M/D/1, D/D/1	BBU	No info	No	No
[9]	MILP, Heuristic	MH/FH Load balance	Static	No	1 user/TTI, 2x2 MIMO, 20 MHz	Yes	No
This work	MILP, Heuristic	Min. energy consumption	Queuing & self-queuing	PP, TN	100 MHz spectrum, 8x8 MIMO, 64QAM	Yes	Yes

DFS: Dynamic Functional Split, **TN:** Transport Network

CU power consumption and DU handovers. A heuristic is also proposed to reduce solving time. In their system model, they assume DU is placed in the cell site with the RU, and limit their system to a single functional split. Even though it is one of the first works to consider RAN energy consumption, they only focus on CU power consumption and ignore DU and RU energy models. Besides, latency and slicing are disregarded.

D. Limitations of Existing Work

Many works propose MILP formulations, which often require considerable computational resources and time to be solved. To address this problem, heuristics and deep reinforcement learning approaches are commonly used to obtain near-optimal solutions more efficiently. In some cases, the MILP model is introduced for completeness, while only the heuristic is evaluated in practice. In contrast, our approach can provide optimal results in substantially less time for small and medium-sized topologies, while a heuristic is introduced to address large scenarios.

RAN energy minimization has been widely studied to reduce RAN OPEX, with different approaches in the literature. Many works focus solely on deactivating processing nodes, often overlooking the energy consumption of network elements such as switches and links. Some works deactivate nodes without explicitly modeling their energy usage. Additionally, several

studies lack of details about their computing models or fail to explain how these models are adapted to different FS. This work explicitly models both processing and network energy consumption, and adopts a transparent, split-aware computing model that aligns VNF computing demands with the selected functional split.

Latency is a critical factor in RAN design, as access networks must operate within strict timing constraints to meet service-level requirements. However, many works either simplify latency using fixed values or focus solely on propagation delay, overlooking queuing effects that impact FS decisions. In this work, we incorporate a detailed latency model based on TSN principles for a packet-based XH. Our modeling approach is transparent and includes queuing behavior and frame prioritization. Furthermore, we analyze the FS selection results to infer relationships between latency and power consumption, an aspect rarely explored in prior studies.

Finally, yet importantly, most proposals are evaluated on small topologies with homogeneous 4G radio configurations such as channel bandwidth (20 MHz), modulation (64 QAM), number of layers (2x2 MIMO), and so on. Nonetheless, actual 5G implementations use heterogeneous radio configurations [33]. Thus, we evaluate our MILP and heuristic in larger scenarios featuring diverse 5G radio configurations.

III. SYSTEM MODEL

Current mobile networks require a flexible RAN to satisfy network requirements of diverse use cases, while reducing the operations costs, mainly due to energy consumption. It can be achieved with a reconfigurable RAN that adapts to the mobile varying demand, thus the network and computing resources are used efficiently to avoid over or under utilization. The RAN flexibility lies in its ability to reconfigure, which includes FS selection, function placement, and routing. The FS selection is a key configuration since it directly impacts the XH bandwidth and latency requirements. Also, VNF placement and PP selection can reduce energy consumption by minimizing the number of active nodes. Conversely, to achieve better latency, specially for FH or URLLC services, RAN functions can be placed closer to the UE, and more efficient paths should be selected. Thus, a sliced RAN is an effective approach to serve all three services (URLLC, eMBB, and mMTC), where each slice has its own configuration to meet their specific requirements.

The proposed model is based on the O-RAN and NGFI architectures, consisting of processing pool (PP) sites and a packet-switched network that supports RAN slicing for the three services mentioned. The general architecture comprises three layers of PPs: regional servers at the edge site, edge servers at the hub site, and RF and PP servers at the cell site as in Fig. 1. The edge site connects to the 5GC and is farther from the UEs. Both regional and edge servers consist of high-capacity PPs and can serve multiple gNBs by hosting and processing their RAN functions as VNFs. In other words, the PPs can accommodate the CU and DU functions of several gNBs. The edge servers located in the hub site, between the cell and edge site, have lower processing capacity than the regional servers. The cell site relies on RF equipment and a low-capacity PP to support both RF and baseband functions, thereby hosting the RU. The scenario considers gNBs with a variety of RF configurations regarding bandwidth, modulation, and so on. Each RU serves a single gNB, which in turn supports three slices: eMBB, URLLC, and mMTC.

The model is designed to satisfy the aggregated demand of a gNB comprising three slices, where each slice has a percentage of the total traffic: 70% corresponds to eMBB, 25% to URLLC, and 5% to mMTC. In terms of latency requirements per slice, eMBB and mMTC latency should not exceed 10 ms, while the

URLLC has a strict delay limit of 250 μ s. Each traffic type is treated as an independent flow, with each slice having its own configuration.

The work focuses on downlink communication, where data flows from the 5GC to the RU located at the cell site. The analysis begins at the 5GC, which connects to the CU via the backhaul—assumed, which we assume as a direct link. Then, the MH, typically located in the pre-aggregation network, connects the CU to the DU via the F2 interface. The FH is the access network between the DU and RU and uses the eCPRI interface. Depending on the VC, either the MH or FH may be omitted. Finally, the XH relies on packet-switched routers linked by high-capacity dark fiber.

A. Virtual Configuration

The 3GPP in [34] describes eight FS options where the RAN protocol stack is distributed as a chain of functions and executed in different PPs. These options were proposed to ease the strict latency and bandwidth demands imposed by earlier C-RAN architecture, which employed FS option 8. This latter option splits the physical and RF functions and transmits continuous IQ (in-phase and quadrature) symbols, which results in a CBR, even when no demand is attended. This transmission requires precise synchronization and signal integrity, with a strict latency limit of 250 μ s.

Although eight FS options are proposed, only the FS options 2, 7, and 6 have gained widespread adoption and standardization [35]. In particular, FS option 2 separates the PDCP and RLC functions, where the PDCP performs header compression and security functions; then it forwards PDCP PDUs to the RLC layer to adjust their sizes according to MAC specifications and reorders them if needed. Meanwhile, the separation between MAC and high-physical (H-PHY or High-PHY) functions is given by the FS option 6. Here, the MAC is responsible for scheduling, resource allocation, and HARQ procedures, sending physical transport blocks (PRBs) to the high-physical function. Then, the HPHY applies channel coding and modulation mapping for over-the-air transmission. This FS option is motivated by the SCF and is being incorporated as a standardized FS by the O-RAN alliance. On the other side, the O-RAN adapted the traditional FS option 7.2 from 3GPP into the FS option 7.2x. While FS option 7.2 scales xhaul bandwidth based on

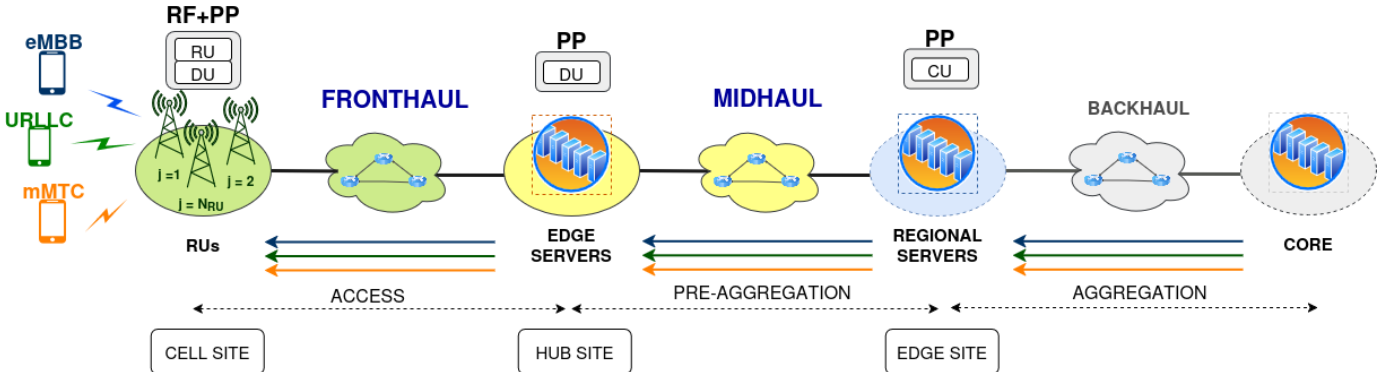


Fig. 1: Employed RAN architecture

TABLE II: Bandwidth and Latency XH Requirements [36]

FS	Bandwidth	Latency
2	$PR \cdot BW / BW_{ref} \cdot NL / NL_{ref} \cdot M / M_{ref}$	10 ms
6	$(PR + CR) \cdot BW / BW_{ref} \cdot NL / NL_{ref} \cdot M / M_{ref}$	250 μ s
7.2x	$2 \cdot 10^{-9}(1 + c) \cdot \frac{v_{NL} \cdot PRB \cdot (12N_{mant} + N_{ex})}{Ts^{\mu}}$	250 μ s

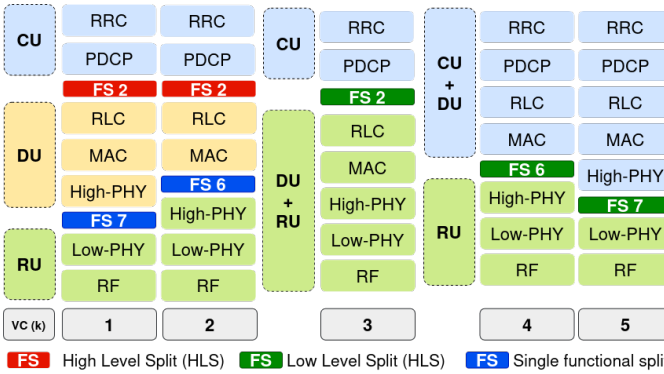


Fig. 2: Virtual configuration options

the number of antennas, FS option 7.2x adjusts it according to the actual demand for PRBs. The bandwidth and latency requirements according to the proposed FS options are included in Table II. The latency requirement of the FS options 2 and 6 are not as strict because their procedures are not time-critical, while the HARQ retransmission has up to 4ms time limit.

The proposed architecture supports single and dual split scenarios based on the selected VC, which defines one or two FS options per gNB and determines the number of nodes required to host the RAN units (CU, DU, and RU). Figure 2 illustrates the set of possible VC options, which can be tailored to each network slice in our model. The figure depicts three representative VC scenarios. The first scenario adopts a dual-split approach, where the CU, DU, and RU are deployed on independent nodes in the PPs and cell-site. In this configuration, both MH and FH links are present: the high-level split between the CU and DU employs a FS option 2, while the low-level split between the DU and RU can use either FS option 7.2x or 6. Alternatively, the following VC options only employ a single functional split, enabling either a MH or a FH. For instance, in VC 3, the DU is placed together with the RU in the cell site, while the MH connects the CU to the DU and RU with a FS option 2. In VCs 4 and 5, the CU and DU are co-allocated in the regional servers and linked to the RU via a FH, employing FS options 6 and 7.2x, respectively.

Each VC option has distinct implications in RAN latency, energy consumption, and computing utilization. First, the placement of PP nodes significantly influences RAN latency due to the distance between nodes: greater distances result in increased delays. Therefore, RAN units should be deployed on closely among nodes or near the RU to satisfy service and XH latency restrictions. Second, the number of active nodes, both PP and network, directly impacts RAN energy consumption. While VCs using only two PPs are more energy efficient, dual-split configurations, despite requiring additional active nodes, may be necessary to meet performance requirements.

B. Computing Model

We adopt the model proposed in [19] and [37] to estimate the RAN computing demands under FS as in [38]. Each function is virtualized and their computing requirements are measured in GOPS:

$$C_{RF} = C_{ref} \cdot \frac{BW}{BW_{ref}} \cdot \frac{A}{A_{ref}} \quad (1)$$

$$C_{LPHY} = C_{ref} \cdot \frac{BW}{BW_{ref}} \cdot \frac{A}{A_{ref}} \cdot \frac{L}{L_{ref}} \quad (2)$$

$$C_{HPHY} = C_{ref} \cdot \frac{BW}{BW_{ref}} \cdot \left(\frac{A}{A_{ref}} \right)^2 \cdot \frac{L}{L_{ref}} \quad (3)$$

$$C_{MAC} = C_{ref} \cdot \frac{BW}{BW_{ref}} \cdot \frac{A}{A_{ref}} \cdot \frac{M}{M_{ref}} \cdot \frac{L}{L_{ref}} \quad (4)$$

$$C_{RLC} = C_{ref} \cdot \frac{A}{A_{ref}} \quad (5)$$

$$C_{PDCP} = C_{ref} \cdot \frac{A}{A_{ref}} \quad (6)$$

$$C_{RRC} = C_{ref} \cdot \frac{A}{A_{ref}} \quad (7)$$

The models consists of reference computing load per function in GOPS C_{ref} based on [39]. BW denotes the carrier bandwidth in MHz, A indicates the number of MIMO antennas, L is the user traffic demand, and M refers to the modulation per RU. In turn, BW_{ref} , A_{ref} , L_{ref} , and M_{ref} denote the reference values given in [40].

C. TSN for X-haul

The IEEE 802.1cm standard [2] provides guidelines to implement Ethernet bridging in FH and MH networks to satisfy TSN requirements. The standard contains the configuration profile A , which implements the *algorithm of zero* as the transmission selection mechanism to prioritize FH and MH traffic on Ethernet networks.

The standard includes the eCPRI interface for low-level splits and the F1 interface for high-level splits within *Class 2*. This Class defines three types of flows, and their latency requirements according to eCPRI classes of service (CoS) [41]. First, the High-Priority Flow (HPF) for fast user plane data, with latency requirement of 25 to 500 μ s. Then, the Medium-Priority Flow (MPF) for slow user plane data, with latency requirement of 1 to 10 ms. Finally, the Low-Priority Flow (LPF) for control and management data, with latency requirement of 100 ms. In this work, the FH traffic is considered as as HPF and the MH is denoted as MPF due to their latency requirements.

The configuration profile A describes bridge delays produced by queuing and self-queuing delay. The profile specifies two type of frames: "golden" and "low-priority" frames. In this work, we map them to HPF and MPF/LPF, respectively. First, queuing delay results from two factors: the transmission of a lower-priority frame selected before the target frame becomes eligible, or the presence of higher-priority frames queued ahead of it. Thus, queuing delay is given by the transmission time d^{tr} of a maximum size of a frame.

The self-queuing delay can be represented as:

$$m_e^f = P_e^f \wedge P_e^{f'}, \quad \forall f, f' \in \mathcal{F}, e \in \mathcal{E} \quad (I-1)$$

First, let's consider $f \in \mathcal{F}$ as XH flows, and $e \in \mathcal{E}$ as the edges in a graph. P_e^f and $P_e^{f'}$ are binary variables that set as 1 if flows f or f' passes through edge e . Then, binary m_e^f tells whether two flows pass over the same edge e in Eq. (I-1).

$$n_e^f = \neg(P_{e'}^f \wedge P_{e'}^{f'}) \wedge m_e^f, \quad \forall f, f' \in \mathcal{F}, e \in \mathcal{E} \quad (I-2)$$

Similarly, in Eq. (I-2), e' refers to the previous link before reaching e , and binary n_e^f is active only when the previous edges of flows f and f' are different, and they are transmitted over current link e .

$$SQ_e^f = d^{tr} \cdot \sum_{i \setminus f}^{\mathcal{F}} n_e^i, \quad \forall f \in \mathcal{F} \quad (I-3)$$

Finally, the self-queuing delay SQ_e^f for flow f in edge e is given by all the interfering flows on edge e that come from different ports and the transmission delay of the packet d^{tr} Eq. (I-3).

D. Energy Consumption Models

This work considers the energy consumption of the PPs and switches. Next, we describe the employed models for both components. The PPs energy consumption model bases on the one presented in [8]:

$$E_{v'} = n_{v'} \cdot (PP_{v'}/CPP_{v'}) \cdot (WPP_{v'}^{full} - WPP_{v'}^{idle}) \cdot T \quad (e-1)$$

where $E_{v'}$ refers to the energy consumption of a PP node v' during an hour, $n_{v'}$ denotes the number of CPUs in the PP. $PP_{v'}$ and $CPP_{v'}$ indicate the computing utilization and total processing capacity of node v' in $GOPS$, respectively, $WPP_{v'}^{full}$ and $WPP_{v'}^{idle}$ represent the power consumption in Watts when the PP is working at 100% capacity, and when it is idle; and T indicates the utilization period.

The switch power consumption model is described in [42], it comprises of three main elements: the chassis, line cards, and active ports. Then the energy consumption is also given considering the utilization period. It is expressed as:

$$W_w = W_w^{chassis} + n_w^{linecard} \cdot W_w^{linecard} + \sum_x^r n_w^{r_x} \cdot W_w^{r_x} \quad (e-2)$$

$$ESW_w = W_w^{chassis} \cdot T \quad (e-3)$$

Where $W_w^{chassis}$ represents the baseline energy needed to power the chassis. The second term captures the energy used by all active line cards, where $n_w^{linecard}$ is the number of linecards and $W_w^{linecard}$ the power per linecard. The summation term reflects the dynamic energy usage of ports transmitting at rates r_x , with $n_w^{r_x}$ representing the number of such ports and W_w^{port} their individual power demands.

IV. OPTIMAL APPROACH

This section describes the MILP formulation to solve the RAN reconfiguration problem. The RAN network is modeled

as a graph $\mathcal{G} = (\mathcal{V}, \mathcal{E})$ where set \mathcal{V} contains all RAN nodes, and \mathcal{E} denotes the set of edges. The \mathcal{V} set is further divided into two main subsets: \mathcal{V}^P for PPs nodes and \mathcal{V}^{SW} for network nodes (XH routers). The PP subset \mathcal{V}^P is composed of two type of nodes: those supporting only upper-layer RAN functions \mathcal{V}^{PP} , and nodes supporting both upper-layer and RF processing, \mathcal{V}^{RU} . The formal description of the sets is as follows: $\mathcal{V} = \mathcal{V}^P \cup \mathcal{V}^{SW}$, $\mathcal{V}^P = \mathcal{V}^{PP} \cup \mathcal{V}^{RU}$, where \mathcal{V}^{PP} is disjoint of \mathcal{V}^{SW} : $\mathcal{V}^{PP} \cap \mathcal{V}^{SW} = \emptyset$. On the other side, the virtual configuration options are denoted with the set \mathcal{K} with $\mathcal{K} = \{1, \dots, 5\}$ corresponding to the configurations shown in Figure 2. Conversely, the gNBs are expressed with the set \mathcal{I} . Also, each gNB i serves three slices j where $j \in \mathcal{D}$, $\mathcal{D} = \{embb, urrlc, mmtc\}$. A complete notation detail is included in Table III.

The model attends the demands $\lambda_{i,j}$ of each slice of every gNB, so the RAN configurations are defined for each gNB-slice pair i, j . First, a virtual configuration option $VC_{i,j,k}$ is selected among \mathcal{K} options. Based on this configuration, RAN units are allocated in PPs nodes $v' \in \mathcal{V}^{PP}$, with the allocation distributed among the $CU_{i,j,k,v'}$, $DU_{i,j,k,v'}$ and $RU_{i,j,k,v'}$ binary variables. Additionally, a node $v' \in \mathcal{V}^{PP}$ can host RAN units of different pair of gNB-slices i, j with no distinction of virtual configuration. For instance, a node $v' \in \mathcal{V}^{PP}$ can support the DU of gNB-slice $a, embb$ with VC 1, while also serving CU-DU of pair $b, mmhc$ with VC 5. On the other hand, the nodes $v'' \in \mathcal{V}^{RU}$ serve only one gNB i and their three slices.

The computing utilization of each RAN unit is calculated with the function $\rho(i, j, k, v, \lambda)$, which considers the demand $\lambda_{i,j}$, the selected VC k , and the RAN unit $v = \{RU, DU, CU\}$. Based on this information, the function aggregates the computing load of the RAN functions assigned to that unit. Then, the total computing load on each node must respect its total processing capacity $CPP_{v'}$, with the CU placement confined to nodes directly connected to the 5GC, as a modeling constraint.

Also, a path option z is selected for both MH and FH segments, their sources and destinations nodes are defined by the variables $CD_{i,j,k,z}^{a,b}$ and $DR_{i,j,k,z}^{b,c}$, respectively. These nodes correspond to the placement of CU, DU and RU units. The shortest paths for z are then computed using Dijkstra's algorithm, with the RAN units as the source and destination. The paths consists of edges $e \in \mathcal{E}$ and they represent a dark fiber link through which the flow of one or more gNB-slice pairs can transmit XH traffic, as long as their transmission capacity is respected C_e . Let the variables $R_{i,j,e}^{MH}$ and $R_{i,j,e}^{FH}$ tell whether gNB-slice transmits MH or FH flow through the edge e . The function $\tau(\lambda_{i,j}, k)$ estimates the XH load based on the FS(s) of the VC k and the demand of the specific gNB-slice.

Additionally, we consider two types of latency per flow: static $SD_{i,j}$ and dynamic $DD_{i,j,e}$. The static latency consists of propagation and store and forward delay, and are calculated with the functions δ^{SF} and δ^{prop} . Conversely, the dynamic latency is composed of queuing $DD_{i,j,e}^Q$ and self-queuing delay $DD_{i,j,e}^{SQ}$. The functions $\delta^Q(i, j, i', j', e)$ and $\delta^{SQ}(i, j, i', j', e)$ check whether flow i', j' uses the same link as flow i, j , and return the corresponding delay based on packet size, as detailed in Subsection III-C. The latency constraints are

TABLE III: Notation Summary

Symbol	Description	Symbol	Description
Sets			
$i \in \mathcal{I}$	Set of RUs.	$j \in \mathcal{D}$	Set of slices: eMBB, URLLC, and mMTC demands/slices, respectively.
$k \in \mathcal{K}$	Virtual configuration options.	$\mathcal{G} = (\mathcal{V}, \mathcal{E})$	RAN graph.
$e \in \mathcal{E}$	Set of edges.	$v \in \mathcal{V}$	Set of nodes.
$\mathcal{V} = \mathcal{V}^{PP} \cup \mathcal{V}^{SW}$	Subset of nodes: PPs and SWs.	$z \in \mathcal{Z}$	Set of paths.
Variables			
$VC_{i,j,k}$	Binary, 1 if VC k is chosen for i, j .	$RU_{i,j,k,v'}$	Binary, 1 if the RU of i, j is located on node v' with VC k .
$DU_{i,j,k,v'}$	Binary, 1 if the DU of i, j is located on node v' with VC k .	$CU_{i,j,k,v'}$	Binary, 1 if the CU of i, j is located on node v' with VC k .
$R_{i,j,e}$	Binary, 1 if the flow of i, j passes through edge e .	$CD_{i,j,k,z}^{a,b}$	Binary, 1 if the path between nodes a and b of i, j with VC k is selected.
$DR_{i,j,k,z}^{b,c}$	Binary, 1 if the path between nodes b and c of i, j with VC k is selected.	L_e	Transmission load on link e carrying XH traffic of i, j .
$SD_{i,j}^{FH/MH}$	Static delay for FH or MH traffic of i, j .	$SD_{i,j}$	Total static delay in the XH of i, j .
$DD_{i,j,e}^{FH-Q}$	FH queuing delay on link e of i, j .	$DD_{i,j,e}^{MH-Q}$	MH queuing delay on link e of i, j .
$DD_{i,j,e}^{FH-SQ}$	FH self-queuing delay on link e of i, j .	$DD_{i,j,e}^{MH-SQ}$	MH self-queuing delay on link e of i, j .
$DD_{i,j,e}^{FH/MH}$	Total dynamic delay of FH/MH traffic of i, j .	$D_{i,j}$	Total XH delay of i, j .
$APP_{v'}$	Binary, 1 if node v' is active supporting a PP.	ASW_w	Binary, 1 if node w is active supporting a switch.
Constants			
$CPP_{v'}$	Computing capacity in GOPS of node v' .	C_e	Transmission capacity in Gbps of edge e .
Functions			
$\rho(i, j, k, v, \lambda)$	Processing load (GOPS) of i, j with VC k considering the aggregated RU demand.	$\tau(\lambda_i, j, k)$	Transmission rate (Mbps) of i, j with VC k in the XH.
$\phi(z, a, b, e)$	Returns if the link e belongs to the path between nodes $a-b$ for i, j .	$\delta^{SF}(e)$	Store-and-forward delay of link e in μs .
$\delta^{prop}(e)$	Propagation delay of link e in μs .	$\delta^Q(i, j, i', j', e)$	Queuing delay on i, j due to i', j' on link e in μs .
$\delta^{SQ}(i, j, i', j', e)$	Self-queuing delay on i, j due to i', j' on link e in μs .	$\omega(z, v', u', w)$	Returns 1 if node w belongs to the path z between nodes v', u' .
$WPP_{v'}$	Energy consumption of node v .	W_w	Energy consumption of node w .

analyzed from both the slice and XH perspectives. The slice latency requirement is service-dependent, spanning from the 5GC to the RU. Meanwhile, the XH latency is determined by the functional split requirements in the FH or MH segments, as outlined in Table II.

The model first solves the energy minimization objective function in 8, which aims at minimizing the energy consumption of PPs and network equipment of the RAN. The model features the deactivation of idle nodes and adopts the energy consumption models from [28] for PPs and [42] for network equipment, as detailed in Section III-D. Additionally, $EPP_{v'}^{infra}$ and ESW_w^{infra} are considered as the infrastructure energy consumption.

$$\sum_w^{V^{SW}} ASW_w \cdot (ESW_w + ESW_w^{infra}) \quad (8)$$

Subject to constraints (9) to (61).

The latter objective function requires linearization due to variable products. The first and second terms in 8 are linearized using the Big-M method. m is a sufficiently large constant that ensures the correct activation of constraints based on the binary variable n corresponding to $APP_{v'}$ or ASW_w . Then q refers to the energy values of $EPP_{v'}^{}$ or ESW_w . The linearization results in ϵ as $y_{v'}$ for $EPP_{v'} \cdot APP_{v'}$, and z_w for $ESW_w \cdot ASW_w$ as in objective function 62:

$$\min \sum_{v'}^{V^{PP}} APP_{v'} \cdot (EPP_{v'} + EPP_{v'}^{infra}) +$$

TABLE IV: MILP

Objective function: energy (62), latency (63), bi-objective (62) and (63)					
VNF Placement					
$\sum_k^{N_{VC}} VC_{i,j,k} = 1$	$\forall i \in \mathcal{I}, j \in \mathcal{D}$	(9)	$\sum_{v''}^{\mathcal{V}^{RU}} RU_{i,j,k,v''} = VC_{i,j,k}$	$\forall i \in \mathcal{I}, j \in \mathcal{D}, k \in \mathcal{K}$	(10)
$\sum_{v'}^{\mathcal{V}^{PP}} DU_{i,j,k,v'} = VC_{i,j,k}$	$\forall i \in \mathcal{I}, j \in \mathcal{D}, k \in \mathcal{K}$	(11)	$\sum_{v'}^{\mathcal{V}^{PP}} CU_{i,j,k,v'} = VC_{i,j,k}$	$\forall i \in \mathcal{I}, j \in \mathcal{D}, k \in \mathcal{K}$	(12)
$RU_{i,j,k,v'} + DU_{i,j,k,v'} + CU_{i,j,k,v'} \leq 1,$	$i \in \mathcal{I}, j \in \mathcal{D}, k \in \mathcal{K}^{DS}, v' \in \mathcal{V}^{PP}$	(13)	$RU_{i,j,k,v'} + CU_{i,j,k,v'} \leq 1,$	$i \in \mathcal{I}, j \in \mathcal{D}, k \in \mathcal{K}^{SH}, v' \in \mathcal{V}^{PP}$	(14)
$DU_{i,j,k,v''} \leq RU_{i,j,k,v''},$	$i \in \mathcal{I}, j \in \mathcal{D}, k \in \mathcal{K}^{SH}, v'' \in \mathcal{V}^{RU}$	(15)	$\sum_{v''}^{\mathcal{V}^{RU}} \sum_k^{\mathcal{K}^{SH}} (DU_{i,j,k,v''} + RU_{i,j,k,v''}) \leq 2.$	$i \in \mathcal{I}, j \in \mathcal{D}$	(16)
$RU_{i,j,k,v'} + DU_{i,j,k,v'} \leq 1,$	$i \in \mathcal{I}, j \in \mathcal{D}, k \in \mathcal{K}^{SL}, v' \in \mathcal{V}^{PP}$	(17)	$CU_{i,j,k,v'} \leq DU_{i,j,k,v'},$	$i \in \mathcal{I}, j \in \mathcal{D}, k \in \mathcal{K}^{SL}, v' \in \mathcal{V}^{PP}$	(18)
$\sum_{v'}^{\mathcal{V}^{PP}} \sum_k^{\mathcal{K}^{SL}} (CU_{i,j,k,v'} + DU_{i,j,k,v'}) \leq 2,$	$\forall i \in \mathcal{I}, j \in \mathcal{D}$	(19)			
Routing					
$\sum_z^{\mathcal{Z}} P_{i,j,k,z} = VC_{i,j,k},$	$\forall i \in \mathcal{I}, j \in \mathcal{D}, k \in \mathcal{K}$	(20)	$CD_{i,j,k,z}^{a,b} \leq P_{i,j,k,z},$	$\forall i \in \mathcal{I}, j \in \mathcal{D}, k \in \mathcal{K}, a, b \in \mathcal{V}^{PP}, z \in \mathcal{Z}$	(21)
$DR_{i,j,k,z}^{b,c} \leq P_{i,j,k,z},$	$\forall i \in \mathcal{I}, j \in \mathcal{D}, k \in \mathcal{K}, b, c \in \mathcal{V}^{PP}, z \in \mathcal{Z}$	(22)	$\sum_a^{\mathcal{V}^{PP}} \sum_b^{\mathcal{V}^{PP}} \sum_z^{\mathcal{Z}} \sum_k^{N_{VC}} CD_{i,j,k,z}^{a,b} = 1,$	$\forall i \in \mathcal{I}, j \in \mathcal{D}$	(23)
$\sum_b^{\mathcal{V}^{PP}} \sum_c^{\mathcal{V}^{PP}} \sum_z^{\mathcal{Z}} \sum_k^{N_{VC}} DR_{i,j,k,z}^{b,c} = 1,$	$\forall i \in \mathcal{I}, j \in \mathcal{D}$	(24)	$\sum_b^{\mathcal{V}^{PP}} \sum_z^{\mathcal{Z}} \sum_k^{N_{VC}} CD_{i,j,k,z}^{a,b} \geq \sum_k^{N_{VC}} CU_{i,j,k,a},$	$\forall i \in \mathcal{I}, j \in \mathcal{D}, a \in \mathcal{V}^{PP}$	(25)
$\sum_k^{N_{VC}} DU_{i,j,k,b},$	$\forall i \in \mathcal{I}, j \in \mathcal{D}, b \in \mathcal{V}^{PP}$	(26)	$\sum_c^{\mathcal{V}^{PP}} \sum_z^{\mathcal{Z}} \sum_k^{N_{VC}} DR_{i,j,k,z}^{b,c} \geq \sum_k^{N_{VC}} DU_{i,j,k,b},$	$\forall i \in \mathcal{I}, j \in \mathcal{D}, b \in \mathcal{V}^{PP}$	(27)
$\sum_b^{\mathcal{V}^{PP}} \sum_z^{\mathcal{Z}} \sum_k^{N_{VC}} DR_{i,j,k,z}^{b,c} \geq$	$\forall i \in \mathcal{I}, j \in \mathcal{D}, c \in \mathcal{V}^{PP}$	(28)	$\sum_i^{\mathcal{I}} \sum_j^{\mathcal{D}} \sum_z^{\mathcal{Z}} \phi(z, a, b, e) CD_{i,j,k,z}^{a,b} = \sum_{P_{i,j,k,e}^{MH}}^{\mathcal{E}}$	$\forall i \in \mathcal{I}, j \in \mathcal{D}, k \in \mathcal{K}, e \in \mathcal{E}$	(29)
$\sum_k^{N_{VC}} RU_{i,j,k,c},$	$\forall i \in \mathcal{I}, j \in \mathcal{D}$	(30)			
$\sum_i^{\mathcal{I}} \sum_j^{\mathcal{D}} \sum_z^{\mathcal{Z}} \phi(z, b, c, e) DR_{i,j,k,z}^{b,c} =$	$\mathcal{D}, k \in \mathcal{K}, e \in \mathcal{E}$				

Continue on the next page

TABLE IV: MILP (cont.)

Link Load			
$\sum_i^{\mathcal{I}} \sum_j^{\mathcal{D}} \sum_k^{N_{VC}} P_{i,j,k,e}^{FH} \cdot \tau^{FH}(\lambda_i, j, k) = L_e^{FH}, \quad \forall e \in \mathcal{E}$	(31)	$\sum_i^{\mathcal{I}} \sum_j^{\mathcal{D}} \sum_k^{N_{VC}} P_{i,j,k,e}^{MH} \cdot \tau^{MH}(\lambda_i, j, k) = L_e^{MH}, \quad \forall e \in \mathcal{E}$	(32)
$L_e = L_e^{FH} + L_e^{MH}, \quad \forall e \in \mathcal{E}$	(33)	$L_e \leq C_e, \quad \forall e \in \mathcal{E}$	(34)
Computing Utilization			
$\sum_i^{\mathcal{I}} \sum_j^{\mathcal{D}} \sum_k^{N_{VC}} (RU_{i,j,k,v'} \rho^{RU}(i, j, k, v, \lambda) \varphi' \in \mathcal{V}^{PP})$	(35)	$PP_{v'} \leq CPP_{v'} \cdot APP_{v'}, \quad \forall v' \in \mathcal{V}^{PP}$	(36)
$DU_{i,j,k,v'} \rho^{DU}(i, j, k, v, \lambda) + CU_{i,j,k,v'} \rho^{CU}(i, j, k, v, \lambda) = PP_{v'},$			
$\sum_k^{N_{VC}} CU_{i,j,k,v'} \leq APP_{v'}, \quad \forall i \in \mathcal{I}, j \in \mathcal{D}, v' \in \mathcal{V}^{PP}$	(37)	$\sum_k^{N_{VC}} DU_{i,j,k,v'} \leq APP_{v'}, \quad \forall i \in \mathcal{I}, j \in \mathcal{D}, v' \in \mathcal{V}^{PP}$	(38)
$\sum_k^{N_{VC}} RU_{i,j,k,v''} \leq APP_{v''}, \quad \forall i \in \mathcal{I}, j \in \mathcal{D}, v'' \in \mathcal{V}^{RU}$	(39)		
Latency			
$SD_{i,j}^{FH} = \sum_e^{\mathcal{E}} \sum_k^{N_{VC}} P_{i,j,k,e}^{FH} (\delta^{SF}(e) + \delta^{prop}(e)), \quad \forall i \in \mathcal{I}, j \in \mathcal{D}$	(40)	$SD_{i,j}^{MH} = \sum_e^{\mathcal{E}} \sum_k^{N_{VC}} P_{i,j,k,e}^{MH} (\delta^{SF}(e) + \delta^{prop}(e)), \quad \forall i \in \mathcal{I}, j \in \mathcal{D}$	(41)
$SD_{i,j} = SD_{i,j}^{FH} + SD_{i,j}^{MH}, \quad \forall i \in \mathcal{I}, j \in \mathcal{D}$	(42)	$R_{i,j,e}^{FH} = \sum_k^{N_{VC}} P_{i,j,k,e}^{FH}, \quad \forall i \in \mathcal{I}, j \in \mathcal{D}, e \in \mathcal{E}$	(43)
$R_{i,j,e}^{MH} = \sum_k^{N_{VC}} P_{i,j,k,e}^{MH}, \quad \forall i \in \mathcal{I}, j \in \mathcal{D}, e \in \mathcal{E}$	(44)	$P_{i,i',j,j',e}^{FH-FH} = R_{i,j,e}^{FH} \cdot R_{i',j',e'}^{FH}, \quad \forall i, i' \in \mathcal{I}, j, j' \in \mathcal{D}, e \in \mathcal{E}$	(45)
$P_{i,i',j,j',e}^{FH-MH} = R_{i,j,e}^{FH} \cdot R_{i',j',e'}^{MH}, \quad \forall i, i' \in \mathcal{I}, j, j' \in \mathcal{D}, e \in \mathcal{E}$	(46)	$P_{i,i',j,j',e}^{MH-MH} = R_{i,j,e}^{MH} \cdot R_{i',j',e'}^{MH}, \quad \forall i, i' \in \mathcal{I}, j, j' \in \mathcal{D}, e \in \mathcal{E}$	(47)
$P_{i,i',j,j',e}^{MH-FH} = R_{i,j,e}^{MH} \cdot R_{i',j',e'}^{FH}, \quad \forall i, i' \in \mathcal{I}, j, j' \in \mathcal{D}, e \in \mathcal{E}$	(48)	$DD_{i,j,e}^{FH-Q} = P_{i,i',j,j',e}^{FH-MH} \delta^{FH-Q}(i, j, i', j', e), \quad \forall i, i' \in \mathcal{I}, j, j' \in \mathcal{D}, e \in \mathcal{E}$	(49)
$DD_{i,j,e}^{FH-SQ} = \sum_{(i',j') \in \mathcal{H}} P_{i,i',j,j',e}^{FH-FH} \delta^{FH-SQ}(i, j, i', j', e), \quad \forall i, i' \in \mathcal{I}, j, j' \in \mathcal{D}, e \in \mathcal{E}$			
$DD_{i,j,e}^{MH-SQ} = \sum_{(i',j') \in \mathcal{L}} P_{i,i',j,j',e}^{MH-MH} \delta^{MH-SQ}(i, j, i', j', e), \quad \forall i, i' \in \mathcal{I}, j, j' \in \mathcal{D}, e \in \mathcal{E}$			
$DD_{i,j,e}^{MH-Q} = \sum_{(i',j') \in \mathcal{H}} P_{i,i',j,j',e}^{MH-FH} \cdot \delta^{MH-Q}(i, j, i', j', e) + P_{i,i',j,j',e}^{MH-MH} \cdot \delta^{MH-Q}(i, j, i', j', e), \quad \forall i, i' \in \mathcal{I}, j, j' \in \mathcal{D}, e \in \mathcal{E}, (i', j') \in \mathcal{L}$			
$D_{i,j}^{MH} = \sum_e^{\mathcal{E}} (DD_{i,j,e}^{MH-Q} + DD_{i,j,e}^{MH-SQ}), \quad \forall i \in \mathcal{I}, j \in \mathcal{D}$			(53)
$DD_{i,j,e}^{FH} = \sum_e^{\mathcal{E}} (DD_{i,j,e}^{FH-Q} + DD_{i,j,e}^{FH-SQ}), \quad \forall i \in \mathcal{I}, j \in \mathcal{D}$			(54)

Continue on the next page

TABLE IV: MILP (cont.)

$D_{i,j}^{MH} = SD_{i,j}^{MH} + DD_{i,j,e}^{MH},$	$\forall i \in \mathcal{I}, j \in \mathcal{D}$	(55)	$D_{i,j}^{FH} = SD_{i,j}^{FH} + DD_{i,j,e}^{FH},$	$\forall i \in \mathcal{I}, j \in \mathcal{D}$	(56)
$D_{i,j} = D_{i,j}^{FH} + D_{i,j}^{MH},$	$\forall i \in \mathcal{I}, j \in \mathcal{D}$	(57)	$D_{i,j} \leq l_{i,j}^{max},$	$\forall i \in \mathcal{I}, j \in \mathcal{D}$	(58)
$D_{i,j}^{MH} \leq l_{i,j}^{MH},$	$\forall i \in \mathcal{I}, j \in \mathcal{D}$	(59)	$D_{i,j}^{FH} \leq l_{i,j}^{FH},$	$\forall i \in \mathcal{I}, j \in \mathcal{D}$	(60)
Energy					
$\sum_{v'}^{\mathcal{V}^{PP}} \sum_{u'}^{\mathcal{V}^{PP}} \sum_z^{\mathcal{Z}} \sum_k^{N_{VC}} \left(CD_{i,j,k,z}^{v',u'} + DR_{i,j,k,z}^{v',u'} \right) \omega(z, v', u', w) \leq ASW_w, \forall i \in \mathcal{I}, j \in \mathcal{D}, w \in \mathcal{V}^{SW}$					(61)

$$\begin{aligned}
\epsilon &\leq m * n & (1-1) \\
\epsilon &\leq q & (1-2) \\
\epsilon &\geq q - (1 - n) \cdot m & (1-3) \\
\epsilon &\geq 0 & (1-4)
\end{aligned}$$

$$\min \sum_{v' \in \mathcal{V}^{PP}} y_{v'} + \sum_{w \in \mathcal{V}^{SW}} z_w \quad (62)$$

Subject to constraints (9) to (61).

The model is then tested for FH latency minimization, a key factor due to the strict delay requirements of URLLC and low-level FS options. The total FH latency is the sum of the FH delay of all pairs of gNB-slices.

$$\min : \sum_i^{\mathcal{I}} \sum_j^{\mathcal{D}} D_{i,j}^{FH} \quad (63)$$

Subject to constraints (9) to (61). Finally, a bi-objective function is applied to balance energy consumption and FH latency. This approach employs a lexicographic method which assigns priorities to each objective and solves them in decreasing order. First, the objective with the highest priority is optimized. Then, the lower-priority objective is addressed, ensuring that its solution preserves the results already achieved for the higher-priority objective. In this case, RAN energy minimization has a higher priority than FH latency minimization due to its impact on OPEX and because the MILP formulation already ensures that latency constraints are met.

$$\begin{aligned}
\min_{x \in X} \quad f_1(x) &= \sum_{v' \in \mathcal{V}^{PP}} y_{v'} + \sum_{w \in \mathcal{V}^{SW}} z_w & (64) \\
\text{s.t.} \quad &\text{Constraints (9) to (61)}
\end{aligned}$$

Let f_1^* be the optimal value of (64).

$$\begin{aligned}
\min_{x \in X} \quad f_2(x) &= \sum_i^{\mathcal{I}} \sum_j^{\mathcal{D}} D_{i,j}^{FH} & (65) \\
\text{s.t.} \quad &f_1(x) = f_1^* \text{ and Constraints (9) to (61)}
\end{aligned}$$

The model constraints range from (9) to (61) and are included in Table IV.

In constraint (9) a unique virtual configuration option k is set for each pair RU-slice i, j with the decision variable $VC_{i,j,k}$. Constraint (10) to (12) configure RAN units (RU, DU, CU) to have a unique VC option k and node v per i, j . In constraint (13),

it is ensured the RAN units are placed in three different nodes for the VC options $k = \{1, 2\}$ where dual split is selected. Then, the expression (14) restricts that the CU is placed in a different node than the RU, while constraints (15) and (16) ensure that both DU and RU are placed in the same node. Similarly, in constraint (17) to (19), for $k = \{4, 5\}$ the DU is placed in the same node as the CU, but separated from the RU.

In constraint (20) a single path z and VC option k are chosen per slice j of RU i . In constraints (21) and (22), the FH and MH paths, which connect nodes a to b and b to c respectively, associate the VC k and path z with the RU-slice pair i, j . The expressions (23) and (24) make sure a single segment is chosen for MH and FH per i, j . In constraints (25) and (26), the source and destination nodes are given for the MH segment of i, j . That is, for MH, a CU node a is considered as source and a DU node b as destination. Likewise, constraints (27) and (28) compose the FH path between the DU node b to the RU node c . Finally, constraints (29) and (30) active a link e if it is part of a RAN segment either MH or FH.

Constraints (31) and (32) calculate the total MH and FH transmission load of i, j , considering the VC k , on link e . In constraint (33) the total transmission load, considering MH and FH loads conveyed through edge e , is estimated, then in constraint (34) that load is constrained to the transmission capacity of the link C_e .

Constraint (35) estimates the total computing load $PP_{v'}$ on node v' considering all the RAN functions placed in it. Constraint (36) ensures the computing capacity on node v' is not exceeded. Constraint (37) to 39 activate the node v' (binary variable $APP_{v'}$) if at least a slice j is placed on it.

In constraints (40) and (41), the total static latency due to propagation and store and forward delay is calculated for both RAN segments FH and MH. Then constraint (42) sums the total static latency of slice j of RU i from the 5GC to the RU. Then, for the dynamic latency, we simplify the notation of the flow of i, j over link e with new variables $R_{i,j,e}^{FH}$ and $R_{i,j,e}^{MH}$ to disconsider its VC in expressions (43) and (44). As explained in the previous section, to determine the queuing and self-queuing delay in the XH, it is necessary to check whether more than one flow (and their type of flow) coincide on a link e . Thus, constraints (45) to (48) perform that verification for two flows, namely, i, j and i', j' . These expressions are conditional and consider all the possible coincidences between MH and FH flows. The conditional operations are performed with a product between decision variables, which leads to non-linearity-ness. The expressions are then linearized with popular

TABLE V: Heuristic Notation Summary

Symbol	Description
$O_{i,j}$	Overall solution structure containing VC, CU, DU, and RU.
$C_{v'}$	Link usage structure containing the total transmission load of e .
\mathcal{R}_e	PP usage structure containing the total computing load of v and its allocated gNB-slices i, j .
\mathcal{N}	Structure containing no working RAN configurations.
\mathcal{V}_{cand}^P	Set of candidate PPs
IT	Number of iterations
P^{CU}	PP node supporting CU
P^{DU}	PP node supporting DU
P^{RU}	PP node supporting RU
X^{VC}	Selected VC
R^{FH}, R^{MH}	FH and MH paths
v	Set of RAN units CU, DU, RU
\mathcal{V}_{cand}^P	Set of candidate nodes to place CU or DU
R^{cand}	Set of candidate paths for FH or MH
$allocated_{path}$	Variable containing list of edges
$path_{score}$	Variable telling how much a path is used
$best_{path}$	Variable containing a selected path based on $path_{score}$
$placed_{node}$	Variable containing a placed node of a RAN unit

product-linearization approach:

$$z_{i,j} = x_{i,j} \cdot y_{i,j}, \quad \text{where } x_{i,j}, y_{i,j} \in \{0, 1\}, \quad (\text{pl-1})$$

$$z_{i,j} \leq x_{i,j} \quad (\text{pl-2})$$

$$z_{i,j} \leq y_{i,j} \quad (\text{pl-3})$$

$$z_{i,j} \geq x_{i,j} + y_{i,j} - 1 \quad (\text{pl-4})$$

The FH queuing delay of i, j on link e is calculated in constraint (49) which takes into account a MH flow coincidence; while the self-queuing delay is given in constraint (50) considering all the FH flows on the same edge. This latter expression sums all the other coinciding FH flows $(i', j') \in \mathcal{H}$. For MH flows of gNB-slice i, j on e , the queuing delay in constraint (52) consists of all concurrent flows of FH $(i', j') \in \mathcal{H}$. Finally, the MH self-queuing delay given in constraint (51) is estimated summing all the MH flows sharing the link e . The expressions 53 and 54 represent the total dynamic latency of i, j in the FH and MH segments, respectively. Similarly, constraint (55) and 56 show the total latency per segment FH and MH of i, j , combining static and dynamic delay. In turn, 57 represents the total latency of i, j from 5GC to the RU, consisting of dynamic and static latency of FH and MH segments. Then, that latency is first constrained by the slice-latency requirements in constraint (58), and by the FH and MH restrictions in constraint (59) and (60).

Expression 61 checks whether a network node w is part of any FH or MH segment. Finally, the energy consumption model for PPs and network equipment in objective function 8 are calculated with the energy models Eq. (e-1) and Eq. (e-2) as explained in previous section.

Algorithm 1: Main Algorithm

```

Input: Network graph  $\mathcal{G}$ , Demand  $\lambda_{i,j}$ , RUs set  $\mathcal{D}$ , Slices set  $\mathcal{I}$ , Virtual Configurations set  $\mathcal{K}$ , Number of iterations  $IT$ 
Output: Placement, VC and routing result in  $O_{i,j}$ , resources utilization  $C_{v'}$ ,  $\mathcal{R}_e$ 
1  $O'_{i,j}, C'_{v'}, \mathcal{R}'_e, \mathcal{N} \leftarrow \text{Configuration}(\mathcal{G}, \mathcal{D}, \mathcal{I}, \mathcal{K})$  /* First RAN configuration
2 while  $\mathcal{N}$  is not empty do /* Re-configure pending gNB-slices
3    $O'_{i,j}, C'_{v'}, \mathcal{R}'_e, \mathcal{N} \leftarrow \text{Configuration}(\mathcal{G}, \mathcal{D}, \mathcal{I}, \mathcal{K}, \mathcal{N})$  /* Energy Optimization
4    $O_{i,j}(P^{CU}, P^{DU}, P^{RU}, X^{VC}, R^{FH}, R^{MH}), C_{v'}, \mathcal{R}_e, \leftarrow \text{Energy}(IT, O_{i,j}, C_{v'}, \mathcal{R}_e, \mathcal{N})$  /* Energy minimization

```

V. HEURISTIC APPROACH

This Section presents a heuristic algorithm as a simpler alternative to the MILP, capable of solving the RAN configuration problem in reduced time. This heuristic performs the selection of VC, unit placement and routing for FH and MH, while meeting the bandwidth, latency and resource utilization constraints. Additional variables are employed and introduced in Table V. and are described along this section. The heuristic consists of three main components: a main algorithm, a RAN configuration selection part, and an energy minimization function. The main algorithm runs the RAN configuration process until all slices are assigned their respective configurations. It then runs the energy minimization function to modify the gNB-slice RAN configurations so that the overall energy consumption is reduced.

The main algorithm, shown in Algorithm 1, first receives the sets of network graph \mathcal{G} , demand $\lambda_{i,j}$, sets of RUs \mathcal{D} , slices \mathcal{I} , and virtual configurations \mathcal{K} as inputs. This algorithm outputs the RAN configurations in $O_{i,j}$, the computing utilization of PP nodes in $C_{v'}$, and the link utilization \mathcal{R}_e of the network. The structure $O_{i,j}$, per pair of gNB-slice i, j contains the unit placement (for CU and DU) with variables P^{CU}, P^{DU} , virtual configurations X^{VC} , and routing R^{FH}, R^{MH} for FH and MH; it is better presented as $O_{i,j}(P^{CU}, P^{DU}, P^{RU}, X^{VC}, R^{FH}, R^{MH})$.

The Algorithm 1 invokes the RAN Configuration function, which returns a first solution containing RAN configurations, and updates the resource utilization of PPs and Links structures. Additionally, it returns \mathcal{N} , a structure that storages no-configured pair of gNB-slices i, j and its corresponding no-working configurations: $P^{CU}, P^{DU}, X^{VC}, R^{FH}, R^{MH}$. Some gNB-slices and their configurations are included in \mathcal{N} due to no compliance of model restrictions and are saved to be ignored in further runs. In Line 2, a loop iterates over the no-allocated slices in \mathcal{N} , so in Algorithm 1 the RAN Configuration can be called again, including to-ignore \mathcal{N} structure. The loop stops only when all gNB-slices are configured, resulting in a first solution. With this first solution, the algorithm invokes the Energy function in Algorithm 1, taking the network graph, slices, virtual configurations, and the results from the previous step ($O_{i,j}, C_{v'}, \mathcal{R}_e$, and \mathcal{N}) as inputs. The function refines the placement, virtual configuration, and routing results to minimize energy consumption while respecting resource constraints. The final optimized outputs, including the updated placement and resource utilization metrics, are returned as $O_{i,j}, C_{v'}$, and \mathcal{R}_e .

The RAN Configuration function in Algorithm 2 per-

Algorithm 2: RAN Configuration Algorithm

Input: Network graph \mathcal{G} , RUs set \mathcal{D} , Slices set \mathcal{I} , Virtual Configurations set \mathcal{K} , PP set \mathcal{V}^P , PP capacity CPP_v
Output: Placement, VC and routing result $O_{i,j}$, resources utilization $C_{v'}$, \mathcal{R}_e , ignored configurations \mathcal{N} , Energy consumption

Init: $C_{v'}$, \mathcal{R}_e
/* RAN Configuration */
1 **if** \mathcal{N} received as argument **then**
2 \mathcal{I} , \mathcal{D} \leftarrow Retrieve i, j elements from \mathcal{N}
3 $O_{i,j}^{ign} \leftarrow$ Retrieve selection of VC, placement and routing elements from \mathcal{N} to be ignored
4 **foreach** $i \in \mathcal{I}$ **do**
5 **foreach** $j \in \mathcal{D}$ **do**
6 $O_{i,j}(P^{CU}, P^{DU}, X^{VC}) \leftarrow \emptyset$, $O_{i,j}(P^{RU}) \leftarrow j$
7 /* Unit Placement */
8 Prioritize virtual configurations \mathcal{K} based on slice type and demand.
9 Retrieve candidate nodes \mathcal{V}_{cand}^P for CU and DU for i, j
10 **foreach** $k \in \mathcal{K}$ **do**
11 /* Perform placement for both units v CU and DU DU */
12 $aux^{cu}, aux^{du}, PP[cu], PP[du] \leftarrow$ Placement
13 $(i, j, k, \mathcal{V}_{cand}^P, v, \lambda_{i,j}, CPP_v)$
14 **if** aux^{cu} AND aux^{du} not empty **then**
15 $O_{i,j}(P^{CU}, P^{DU}, X^{VC}) \leftarrow aux^{cu}, aux^{du}, k$
16 $C_{v'} \leftarrow PP[cu], PP[du]$ Update placement and computing utilization.
17 /* Routing */
18 **foreach** $i \in \mathcal{I}$ **do**
19 **foreach** $j \in \mathcal{D}$ **do**
20 $O_{i,j}(R^{FH}, R^{MH}, SD, DD) \leftarrow \emptyset$
21 /* Perform routing for FH and MH segments */
22 $aux^{FH}, aux^{MH}, L_e^{FH}, L_e^{MH} \leftarrow$ Routing
23 $(\mathcal{G}, i, j, k, segment, O_{i,j}(P^{CU}, P^{DU}, P^{RU}))$
24 **if** aux^{FH} AND aux^{MH} not empty **then**
25 $O_{i,j}(R^{FH}, R^{MH}) \leftarrow aux^{FH}, aux^{MH}$ Update routing
26 $\mathcal{R}_e \leftarrow L_e^{FH}, L_e^{MH}$ Update link usage
27 **else**
28 Add configuration $(i, j, k, aux^{FH}, aux^{MH})$ in ignored \mathcal{N}
29 Update computing usage $C_{v'}$ regarding i, j, k
30 Calculate static and dynamic SD, DD latency per i, j
31 **return** $O_{i,j}, C_{v'}$, $\mathcal{R}_e, \mathcal{N}$

forms RAN configuration, including the CU and DU placement, virtual configuration selection, and FH and MH routing.

Its first line checks whether any ignored configurations \mathcal{N} were passed as an argument. In that case, Algorithm 2 retrieves the set of pair gNB-slice i, j to be re-allocated from the structure \mathcal{N} . Then, line Algorithm 2 retrieves the RAN configurations $O_{i,j}^{ign}$ to be skipped in further lines.

Then, an iteration begins for each gNB $i \in \mathcal{I}$ and slice $j \in \mathcal{D}$ in to allocate RAN configurations. In Algorithm 2 the $O_{i,j}$ structure for P^{CU}, P^{DU} and X^{VC} is initialized as empty for i, j ; in the case of $O_{i,j}(RU)$, its gNB cell-site is allocated. In Algorithm 2, the \mathcal{K} is organized according to the slice i . For instance, for eMBB slices, the set \mathcal{K} would remain since it might need three PPs due to their high demand and computing requirements; while for URLLC slices, VC options k where the DU is closer to the cell-site are prioritized; and mMTC slices would prioritize single-split configurations since their computing requirements are lower. Next, in Algorithm 2, candidate nodes \mathcal{V}_{cand}^P for P^{CU} and P^{DU} are retrieved according to the distance to the cell-site and node usage percentage: the closer

and more used are prioritized. Line 38 iterates over the set of ordered VC options $k \in \mathcal{K}$ per slice. Algorithm 2 calls Placement function to get the temporal allocation of CU and DU nodes with $aux^{cu}, aux^{du} \in \mathcal{V}^{PP}$, and the temporal total computing utilization of these nodes $PP[cu], PP[du]$. After that, the temporal allocation is verified to be possible, if so, the overall result and computing utilization structures are updated in Algorithm 2.

The (placement and routing) functions are included in Algorithm 3 and detailed as follows. The Placement function, shown in Lines 1 to Algorithm 3, returns the allocation nodes for CU and DU and ensures the computing capacity is constrained. It starts by calculating the processing load $ppload$ required for each RAN unit using the $\rho(i, j, k, v, \lambda)$ function Algorithm 3. In Line 3, the algorithm iterates over the candidate nodes to hold the DU or CU. In Algorithm 3, the total computing load of the candidate node is calculated PP_{vcand} considering the current load plus the required load $ppload$. Then, it is verified that the computing utilization respects the computing capacity in Algorithm 3. If so, the RAN unit is placed on the candidate node Algorithm 3. Otherwise, the node is considered unsuitable and $placed_node$ is marked as empty Algorithm 3. Finally, the $placed_node$ is returned.

After the placement steps, the routing phase starts in Line 12 by iterating over each gNB and slice to be allocated with FH and MH paths. Algorithm 2 initializes the $O_{i,j}$ structure for the FH, MH path selection and their both static and dynamic latencies SD and DD per i, j . The Routing function is called for both segments FH and MH in Algorithm 2, it returns the selected FH and MH paths aux^{FH}, aux^{MH} and the transmission load of the edges of the paths $\mathcal{R}_e \leftarrow L_e^{FH}, L_e^{MH}$.

The Routing function, as defined in Lines 12 to Algorithm 3, selects and returns the paths for both FH and MH segments. It starts by retrieving the source and destination nodes based on *segment* (whether FH or MH) from the $O_{i,j}(CU, DU, RU)$ structure Algorithm 3. Then, it computes possible paths using Dijkstra's algorithm Algorithm 3. For each candidate path, the function calculates the static latency $SD_{i,j}$ Algorithm 3. If the latency is within the acceptable range, Algorithm 3 calculates the required transmission load L_e^{temp} for each edge in the path with function $\tau(\lambda_i, j, k)$. In Algorithm 3, the total transmission load in the edge L_e^{cand} is calculated by adding the load of the current edge L_e^{temp} to the existing link usage \mathcal{R}_e . The load L_e^{cand} is compared to the link capacity C_e , and if the path's load is within capacity, the path is allocated Algorithm 3. Otherwise, *allocated_path* is assumed empty Algorithm 3. If no valid path r^{cand} is found, *allocated_path* is also assigned as empty Algorithm 3. In Algorithm 3, the *allocated_path* is given a score based on the number of slices passing over nodes in the path: the more slices, more score is assigned. Then, in Algorithm 3, the best path *best_path* is updated with the path with the highest score. The variables *best_path* and transmission load L_e^{cand} are then returned in Algorithm 3.

The Energy Minimization function, as defined in Lines 1 to 19, aims at minimizing the overall energy consumption of the RAN while respecting the model constraints. The function receives a specific number of iterations IT , and the first solution structures, namely, $O_{i,j}, C_{v'}$ and \mathcal{R}_e , also the no-

Algorithm 3: Configuration Functions

Input: Network graph \mathcal{G} , RUs set \mathcal{D} , Slices set \mathcal{I} , Virtual Configurations set \mathcal{K} , PP set \mathcal{V}^P , PP capacity $CPP_{v'}$
Output: Placement, VC and routing result $O_{i,j}$, resources utilization $C_{v'}$, \mathcal{R}_e , ignored configurations \mathcal{N} , Energy consumption

Init: $C_{v'}$, \mathcal{R}_e

1 Function Placement ($i, j, k, \mathcal{V}^P_{cand}, v, \lambda_{i,j}, CPP_{v'}$) :

$pP_{v,cand} \leftarrow$ Calculate unit processing load with $\rho(i, j, k, v, \lambda)$

foreach v^{cand} in \mathcal{V}^P_{cand} **do**

$PP_{v,cand} \leftarrow pP_{v,cand} + C_{v,cand}$

if $PP_{v,cand} \leq CPP_{v'}$;

then

$placed_node = v^{cand}$

else

$placed_node = \text{None}$

return $placed_node, PP_{v,cand}$

11 Function Routing ($\mathcal{G}, i, j, k, segment, O_{i,j}(P^{CU}, P^{DU}, P^{RU})$) :

$src, dest \leftarrow$ Retrieve source and destination from $O_{i,j}(P^{CU}, P^{DU}, P^{RU})$

$R^{cand} \leftarrow \text{dijkstra}(\mathcal{G}, src, dest)$

$best_path \leftarrow \text{None}$

foreach r^{cand} in R^{cand} **do**

$SD_{i,j} \leftarrow$ Calculate static latency

if $SD_{i,j} \leq l_{i,j}^{max}$ **then**

foreach e in r **do**

$L_e^{tmp} \leftarrow$ Calculate transmission load with $\tau(\lambda_{i,j}, k)$

$L_e^{cand} \leftarrow L_e^{tmp} + \mathcal{R}_e$

if $L_e^{tmp} \leq C_e$ **then**

$allocated_path = r^{cand}$

else

$allocated_path = \text{None}$

else

$allocated_path = \text{None}$

$path_score \leftarrow \text{score}(allocated_path)$ If the path edges are already used

$best_path \leftarrow allocated_path$ Path with best score

return $best_path, L_e^{cand}$

working configurations \mathcal{N} . It begins by calculating the initial energy consumption of the system Algorithm 4. The function then iterates over the given number of iterations IT , sorting the PP utilization in descending order $C_{v'}^{ord}$ to prioritize the least used processing pools in Algorithm 4.

For each PP v^{cand} in the PP sorted list, in Algorithm 4 the gNB-slices i, j allocated to the PP and their current configurations are retrieved into $\mathcal{S}_{i,j}^{ord}$.

Then, for each retrieved slice $s_{i,j}$, Algorithm 4 saves backups of the current solutions. Thus if the re-configuration does not produce an improvement, the algorithm can roll back to the previous working configuration. In Algorithm 4, a backup is also performed for \mathcal{N} and the current configuration is included to not be repeated in the next configuration step. In Algorithm 4, the gNB-slice elements are retrieved as sets to be reconfigured. Algorithm 4 invokes the Configuration function, updating the $O_{i,j}$, $C_{v'}$, and \mathcal{R}_e structures. If no configurations are pending during the process, the new solution $O'_{i,j}$ (only $\mathcal{I}', \mathcal{D}'$) is included to the previous one in Algorithm 4. After that, the new energy consumption W'_v is calculated in Algorithm 4. If the new energy consumption is lower than the previous value, Algorithm 4 updates the PP and link utilization with the new values. If configurations are not reconfigured successfully Line 17, the algorithm rolls back to the backup state, restoring the previous configurations Algorithm 4. The function

Algorithm 4: Energy Minimization

Input: Demand $\lambda_{i,j}$, PP capacity $CPP_{v'}$, Link capacity C_e
Output: RAN configuration $O_{i,j}$, PP utilization $C_{v'}$, Link utilization \mathcal{R}_e , ignored configurations \mathcal{N} , Energy consumption W_v

1 Function EnergyMin ($IT, O_{i,j}, C_{v'}, \mathcal{R}_e, \mathcal{N}$) :

2 Calculate overall RAN energy W

3 foreach it in IT **do**

$C_{v'}^{ord} \leftarrow C_{v'}$ Order descending less used PPs

foreach $v^{cand} \in C_{v'}^{ord}$ **do**

$S_{i,j}^{ord} \leftarrow v^{cand}$ Retrieve slices i, j in v^{cand}

foreach $s_{i,j} \in S_{i,j}^{ord}$ **do**

 /* Save backup of working solutions */

$O''_{i,j} \leftarrow O_{i,j}$, $C''_{v'} \leftarrow C_{v'}$, $\mathcal{R}''_e \leftarrow \mathcal{R}_e$

$N'' \leftarrow \mathcal{N}, O_{i,j}$ Copy and include slice configs.

$\mathcal{I}', \mathcal{D}' \leftarrow s_{i,j}$ Retrieve i, j elements

$O'_{i,j}, C'_{v'}, \mathcal{R}'_e, N' \leftarrow \text{Configuration}(\mathcal{G}, \mathcal{D}, \mathcal{I}, \mathcal{K})$

if N' empty **then**

$O_{i,j} \leftarrow O'_{i,j}$ Update complete solution

 Calculate new RAN energy consumption $W'_v(O_{i,j})$

if $W'_v < W_v$ **then**

$C_{v'} \leftarrow C'_{v'}$, $\mathcal{R}_e \leftarrow \mathcal{R}''_e$ Update PP and link utilization

else

 /* Roll back to backup */

$O_{i,j} \leftarrow O''_{i,j}$, $C_{v'} \leftarrow C''_{v'}$, $\mathcal{R}_e \leftarrow \mathcal{R}''_e$

return $O_{i,j}, C_{v'}, \mathcal{R}_e$

TABLE VI: Solving time per MILP scenario

Topology	Average solving time [s]		
	Energy Min.	Latency Min.	Bi-objective
Hierarchy	345	308	320
Mesh	3254	3643	3324

continues iterating until all the possible slice placements have been evaluated. Finally, the algorithm returns the optimized configuration, along with the updated PP and link utilization in Algorithm 4.

VI. PERFORMANCE EVALUATION

This section presents the results of the evaluation of the proposed MILP and heuristic in two different realistic scenarios. First, we describe the evaluating scenarios and characteristics of the elements in the RAN system such as resource capacities and RF parameters. Then, different results are discussed and compared among topologies and the three objective functions. First, the virtual configuration selection is analyzed to observe its behavior per slice. Next, the RAN energy consumption and latency are compared among objective functions and heuristic, highlighting their trade-off. Finally, the computing usage of PPs is examined to identify relationships between VC selection and demand. All results are presented on an hourly basis.

A. Scenario Description

Two type of topologies are used to evaluate our model: a hierarchical and a mesh as shown in Fig. 3. The first topology is based on the Passion project [43]; while the second, the mesh one, bases on [25], representing a real implementation. Both

TABLE VII: Link capacities

Link type	Capacity [Gbps]
Router - Router	100
Router - PP	200
PP - RU	25
PP - PP	200

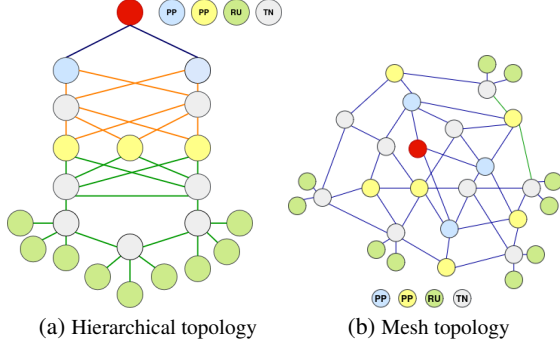


Fig. 3: Topologies

types of topologies follow the guidelines in [35] regarding access and aggregation architectures.

The topologies are represented as graphs in Fig. 3 where each node can perform as either PP or router. Green nodes represent cell sites where RUs are placed, they support RF and processing functions. Yellow and blue nodes symbolize PPs, while gray nodes denote routers. Finally, the red node represents the 5GC. The PPs count on a set of Xeon Gold 6140 processors [29], each with a computing capacity of 864 GOPS [44]. In the experiments, the blue nodes consist of 5 processors, while the yellow nodes and RUs contain 2 processors. According to [45], Intel Xeon Gold 6140 processor can consume approximately 343 Watts of power on average when operating under full computational load, and 52,4 Watts when idle. Conversely, the chassis power consumptions is 940 Watts, the linecard consumes 1170 Watts and 3,5 Watts per port [46].

The FH and MH utilize Ethernet links and their transmission capacities are presented in Table VII as in [25], and their optical length base on Passion project. The propagation delay is $5\mu\text{s}/\text{km}$, store-and-forward delay of $5\mu\text{s}$, and the Ethernet-packet sized used is 1542 Bytes.

We evaluate our model in a realistic 5G RAN scenario using RF settings from real deployments [33], and standards like TS 36.213. As in [33], standalone RAN implementations use diverse RF configurations for RUs. Key RF configuration parameters include channel bandwidth (BW), modulation (Mod), antenna configuration (NL), and numerology (μ). The coding rate (R) and the number of physical resource blocks (PRB) were retrieved from [47]. Finally, Table VIII shows the RF configuration of the RUs in both topologies.

We retrieved the aggregated demand per gNB from a dataset of Ireland in [48], which includes gNB locations and peak traffic demand for urban gNBs. To reflect the fluctuating traffic, we adapted the dataset by applying the normalized daily traffic pattern from [49]. This pattern provides hourly demand changes,

TABLE VIII: Configurations per RU

% RUs	BW	Mod	NL	R	PRB	μ	N_{SC}
50	100	264	8	1/3	273	1	3276
40	40	64	4	3/4	100	1	1200
10	20	64	4	2/3	100	0	1200

with significant fluctuations occurring in only 14 hours. Thus, for each topology and objective, the MILP was executed 14 times, corresponding to the observed varying hours. The average MILP solving time is presented in the table VI.

B. Virtual Configuration Selection

Nine heatmaps are presented per topology in Figs. 4 and 5 where each of them refers to an objective function and to a specific slice. The heatmaps show the gNBs' VC selection per hour, where each hour (x-axis) shows the number of RUs choosing a VC option (y-axis) as a square. The squares' intensity vary depending on the number of RUs choosing a specific option: the temperature bar indicates the color matching the quantity of RUs.

For the hierarchical topology, Fig. 4a shows that the selection of VCs for energy minimization results in a more heterogeneous pattern compared to the other objectives. During low and medium demand hours (1h to 15h), centralized options such as VC 4 and VC 5 are mostly chosen, specially for eMBB and URLLC slices, where the CU and DU are co-allocated. Additionally, for mMTC slices, whose demand is the lowest, the distributed VC 3 is often selected where the DU is placed alongside the RU, particularly for RUs with 20 MHz channels. This occurs because VCs 3 to 5 coallocate the DU with either the CU or the RU, requiring only two active nodes to process the RAN stack and thus reduce the overall energy consumption.

In contrast, during high-demand hours (15h to 0h), a dual-split VC is preferred with options 1 and 2. Especially for RUs with 100 MHz channels or eMBB slices using 40 MHz, which require more computing resources. In such cases, the DU is offloaded to a separate node to better distribute the processing load.

Differently, for the FH minimization objective Fig. 4b, two options are the most frequent among the three slices: VC 1 and 3. The reason is that the VC 3 directly makes the FH latency 0, since the DU and RU are co-allocated. Meanwhile, VC 1 is often selected by RUs with higher-channel bandwidth, as their DU load exceeds the cell-site capacity. In such cases, a third node is required, and choosing a nearby PP helps reduce the FH latency.

Finally, the bi-objective results in Fig. 4c show an in-between behavior that combines energy and latency approaches. VC 3 is common, particularly for URLLC and mMTC slices, for two reasons: it contributes to both the reduction of active nodes and FH latency, and these slices require less computing loads then the cell-site can support them. Conversely, VC 5 remains selected to centralize the DU for high-bandwidth channel gNBs, mostly in low-demand hours. During peak-demand hours, VC options 1 and 2 are chosen to offload the DU.

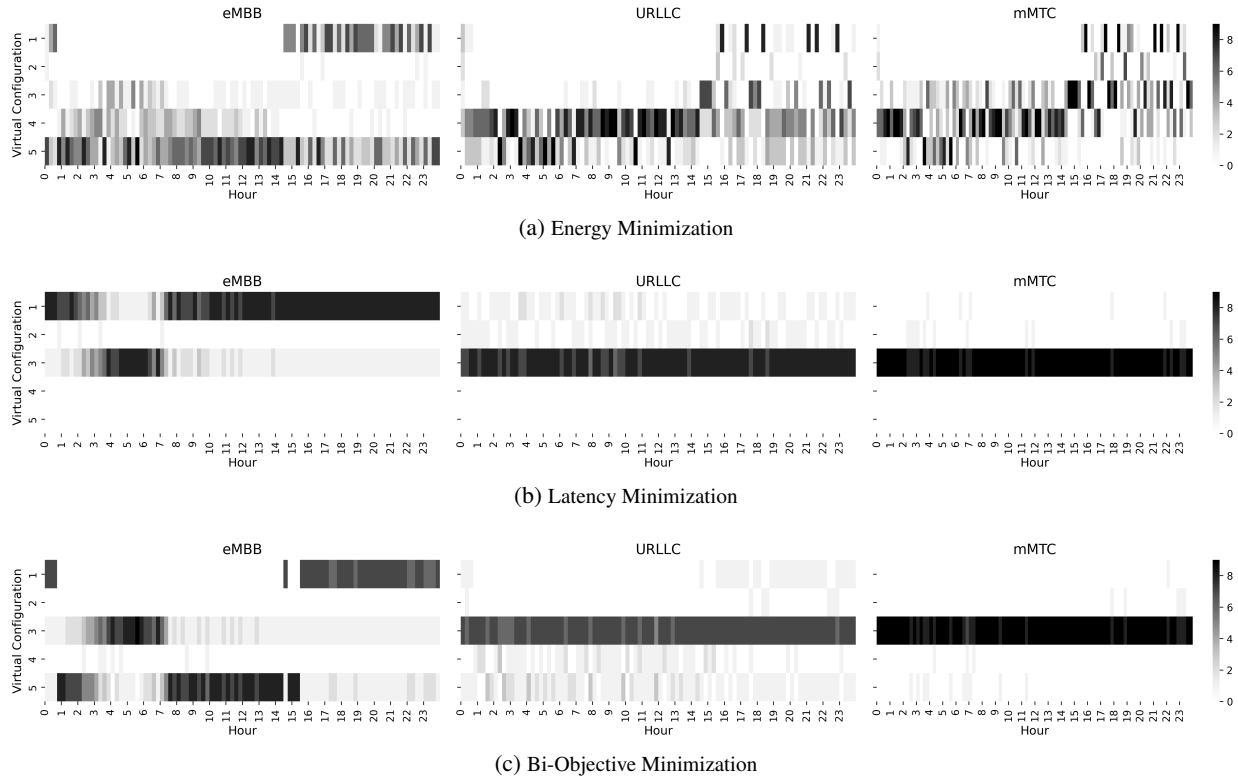


Fig. 4: VC Selection for Hierarchical Topology

At first sight in Fig. 5, the VC selection varies only for the energy objective results between topologies, and for FH latency minimization and bi-objective are similar between topologies. In the first case, for energy minimization Fig. 5a, different from the hierarchical topology, there is no preferred VC and single split configurations are not preferred either; however, options 1, 3, and 5 are more frequent in all the slices. In this topology, even VC that require three active nodes are common because more high-capacity PP nodes are closer to the RU and can support independent DUs. For the latency minimization objective Fig. 5b and bi-objective Fig. 5c, they follow a similar pattern as in the hierarchical topology since VC 5 neglects FH latency and VC 1 and 5 require less active nodes. However, VC 1 is slightly more common than in the hierarchical approach, since PP nodes are closer to the cell sites, latency requirements become less critical when selecting the placement of the CUs and DUs.

C. Energy consumption

Fig. 6 shows the RAN energy consumption of both topologies, and each sub-figure shows the results of the three objectives functions and of the heuristic. It exhibits that the model with energy minimization (green) has significantly lower energy consumption than the model with the latency minimization as objective (orange), but almost similar to the bi-objective (blue), and the heuristic result (purple) shows a balance between energy and latency.

In the hierarchical topology, the difference of energy consumption between energy and latency objectives is approximately 38% for all hours, while the energy consumption difference with the bi-objective is almost negligible as they are

almost overlapped. This constant difference (energy vs latency) is because the hierarchical topology is layered and this leads to structured paths and consistent VNF placement and resource allocation. This also indicates that both RAN configurations in hierarchical topologies (regarding energy minimization and bi-objective) do reduce energy consumption in similar proportions, but the bi-objective approach also benefits from reducing FH latency as seen further in Fig. 7. Regarding the heuristic results, in the hierarchical topology, it shows a ranges from 3% to 36% with respect to energy minimization results, but often lower than latency-objective results. The results are similar especially in low-demand hours, but different in high demand hours.

On the other side, for the mesh topology, the variations of energy consumption between energy and latency objectives range from 4% up to 64% because the results focus merely on latency minimization thus requiring more computing resources and disregarding energy consumption. For the bi-objective, there is a constant energy consumption difference of 16% with respect to the energy minimization objective results. Finally, the mean difference with respect to the heuristic is 5% with a constant behavior. This is a consequence of a more flexible topology since there are more options of paths and VNF allocation per RU. It shows that the trade-off between energy and latency increases in mesh topology.

D. Latency

Figures 7 and 8 illustrate the FH (straight) and MH (dotted) latency behavior for each slice in both hierarchical and mesh topologies trying three different objective functions. The CDFs account for the latencies of RUs' slices over all considered

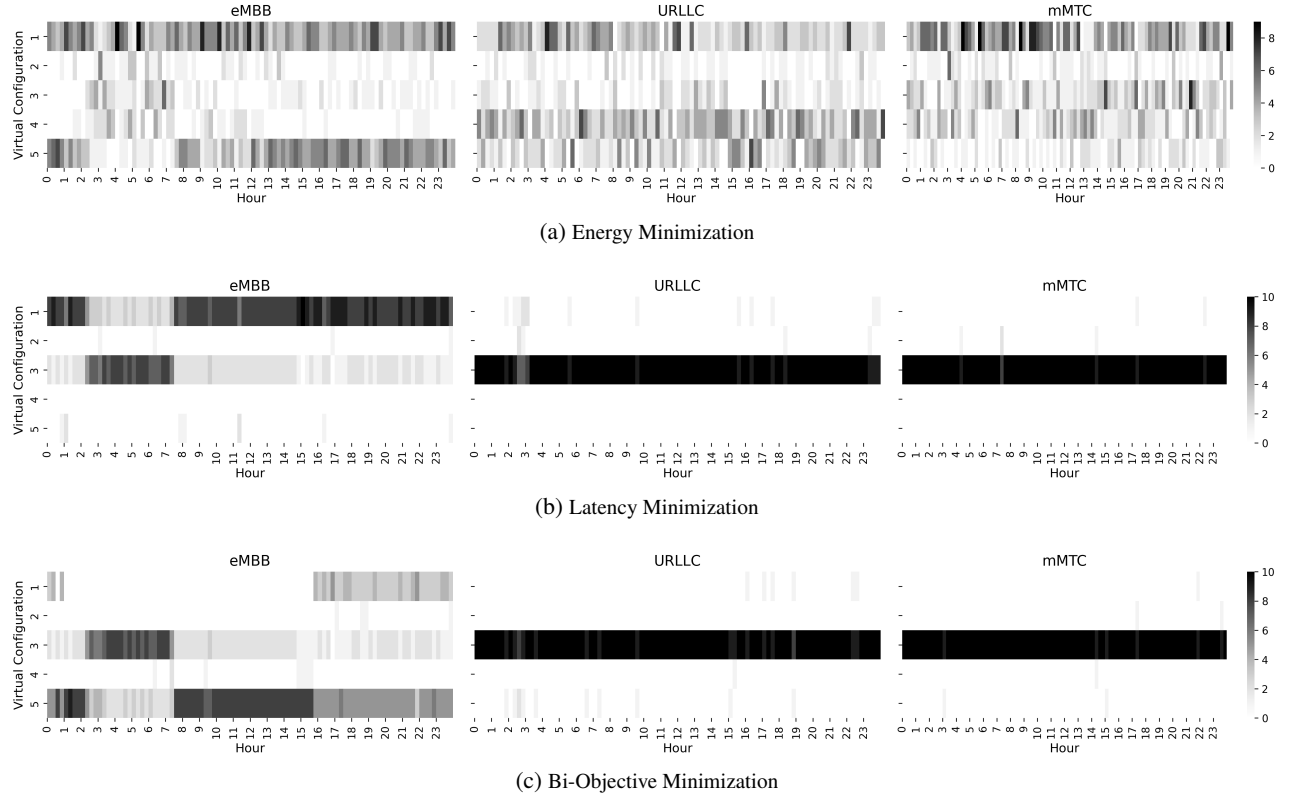


Fig. 5: VC Selection for Mesh Topology

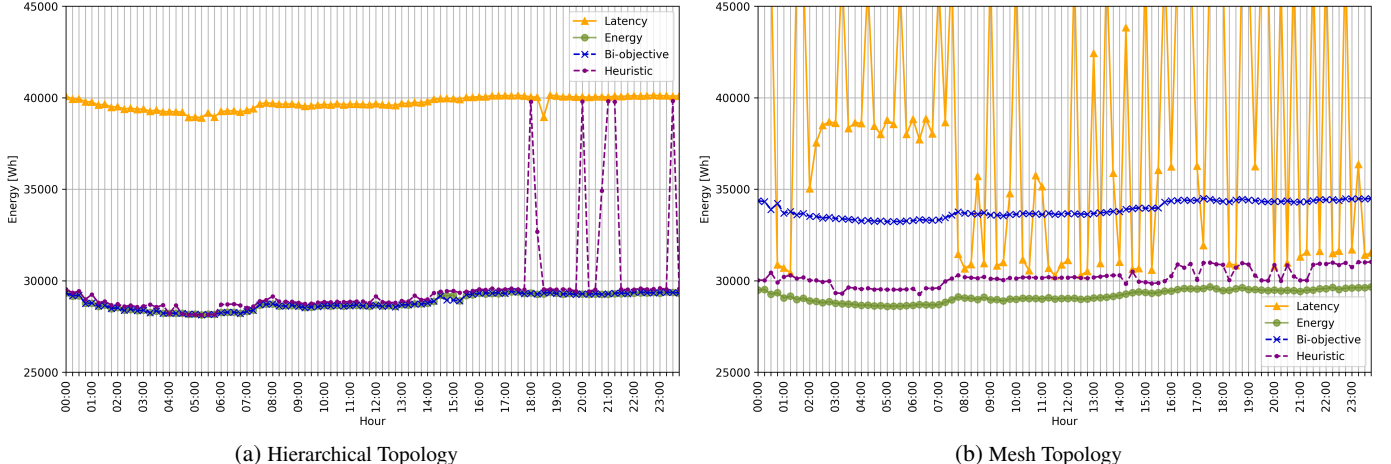


Fig. 6: Energy consumption

hours of the day. As expected, the results of the FH latency minimization objective exhibit the lowest FH latency across all three objective functions. In contrast, energy minimization leads to higher FH delays, and the bi-objective results fall in between. This can be explained by the behavior of the objectives, as well as the impact of the virtual configuration selection.

First, in the energy objective, many slices are centralized on a few nodes (VC options 4 or 5) to minimize the number of active nodes, which leads to an increase in FH latency and low MH latency. It can be seen in both topologies that the MH latency is 0s for at least 30% of all the slices. On the other side,

the hierarchical topology reaches more MH latency (more than $250 \mu s$) due to VC 1 and 3, where the RAN load needed to be distributed into a third node for the DU. Regarding the FH latency in the mesh scenario, it reaches up to $254 \mu s$ because there are closer PP nodes to the RUs where the VNFs can be centralized.

Then, for the FH latency minimization objective, we observe different behaviors with respect to the energy minimization. The FH and MH latency behavior were interchanged: the FH latency decreases while the MH latency increases. At least 25% and of the FH latency is negligible for eMBB slices and 85% for

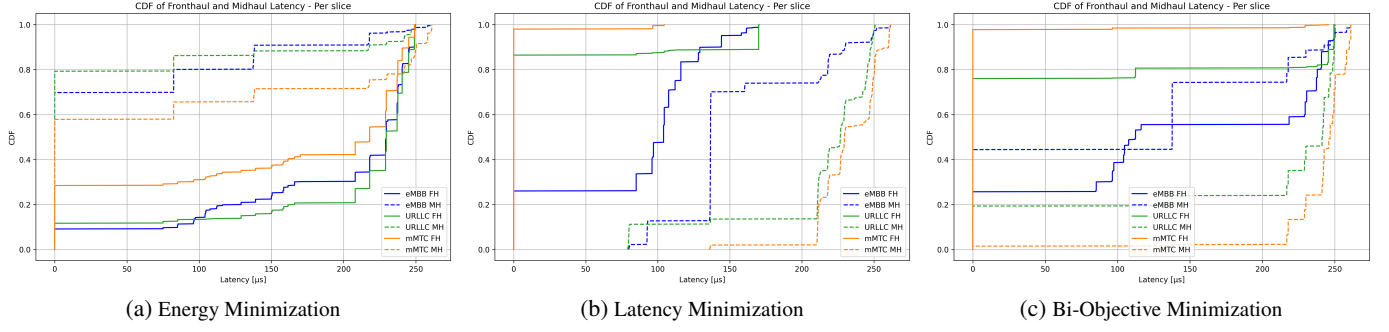


Fig. 7: CDF of End-to-End Latency for the Hierarchical Topology

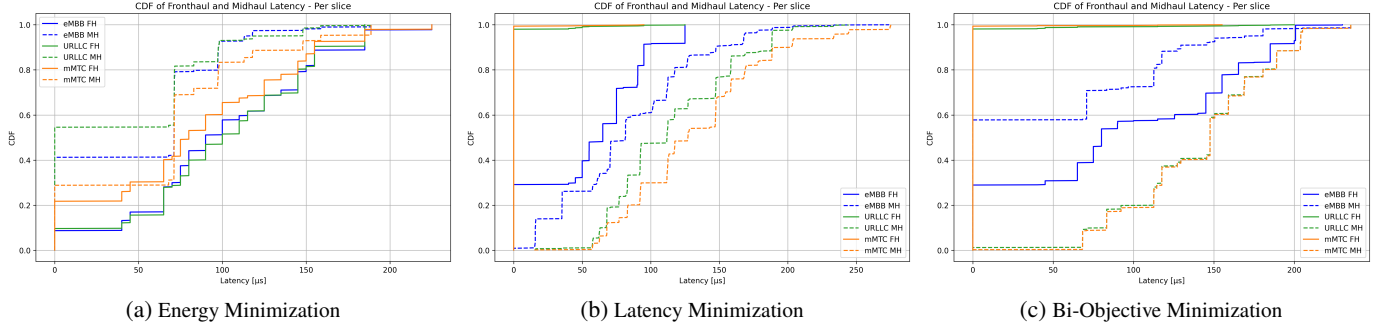


Fig. 8: CDF of end-to-end Latency for Mesh Topology

URLLC and mMTC due to the selection of VC 3, where RU and DU are coallocated. Also, the maximum FH latency reaches to 170 and 130 μ s in the hierarchical and mesh topologies respectively; while in the energy minimization they reach the limit 250 μ s. Due to the VC selection, the MH increased to more than 250 μ s, mainly for mMTC and URLLC whose functions were mostly placed in the cell-site.

Finally, for the bi-objective results, both topologies present similar behavior since the VC selection is similar. In both cases, a significant percentage of the FH latency is 0, specially for URLLC and mMTC, where the VC 3 is common. eMBB FH latency is higher and it shows that this type of slices tend to choose centralized or distributed VC options instead (VC 1, 4 and 5). With this eMBB's behavior, it can be noticed how the computing load impacts in the VC selection. While lighter computing-demanding slices can assume VC 3, the heavier ones (eMBB or slices on 100 MHz RUs), need to distribute the RAN processing in more PP nodes.

E. Computing Usage

The computing utilization is also presented as heatmaps, where the *x-axis* represents the hour of the day and the *y-axis* indicates the PP node numbers. Only PP nodes are analyzed. Each square shows the percentage of total utilization per node at each hour. Figures 9 and 10 show the results for hierarchical and mesh topologies.

The results for energy minimization show that most functions are centralized on high processing nodes, located closer to the 5GC (nodes 1 to 3). Yet, during periods of increased demand, PP nodes with lower computing capacity are occasionally utilized

to support DU functions, and the rest of nodes remain inactive. In contrast, the latency minimization objective results in more active PP nodes, even some with low usage. The reason behind this is that the DUs are placed in independent nodes closer to the RUs. This suggests that minimizing latency requires greater computing resources and hence more active nodes. Finally, the results for the bi-objective function follow a pattern similar to energy minimization, but with slightly variance in the mesh topology. In the hierarchical topology, the structured layout repeatedly selects the same closer-to-RU PPs, yielding the same node selection. In the mesh, the looser structure leads to several placements options, so the active PP nodes are more distributed than in the energy results (more centralized).

VII. CONCLUSION

In this work, we address the RAN configuration problem to minimize overall energy consumption while meeting bandwidth and latency requirements. The proposed approach models the energy consumption of the RAN's PPs and switching devices, ensuring that bandwidth and latency constraints are met. We formulate a MILP model and propose a heuristic method that jointly considers VC selection, VNF placement, and per-slice routing. The evaluation includes three slice types—eMBB, URLLC, and mMTC—each with distinct bandwidth and latency requirements. Additionally, we incorporate FH and MH latency constraints, considering both queuing and self-queuing latency as prescribed by TSN standards. The heuristic provides near-optimal energy solutions with significantly reduced computation time. We analyze various topologies and radio configurations, presenting in-depth results to reveal how VC selection influences

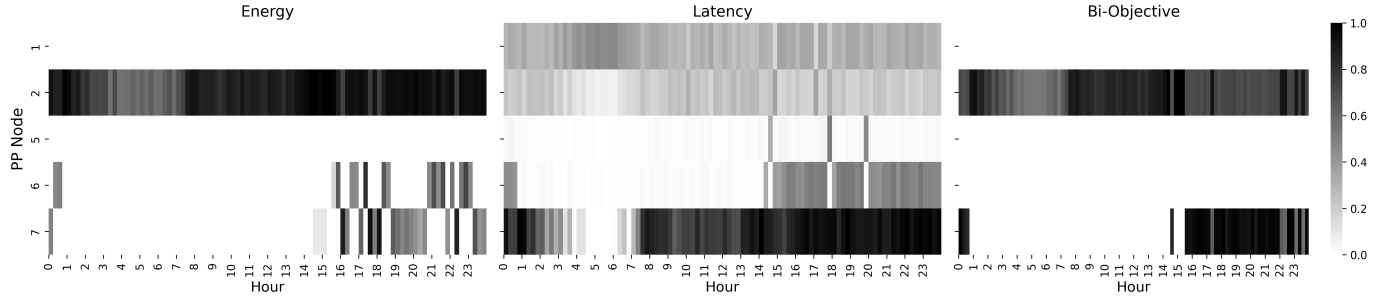


Fig. 9: PP computing utilization for the Hierarchical Topology

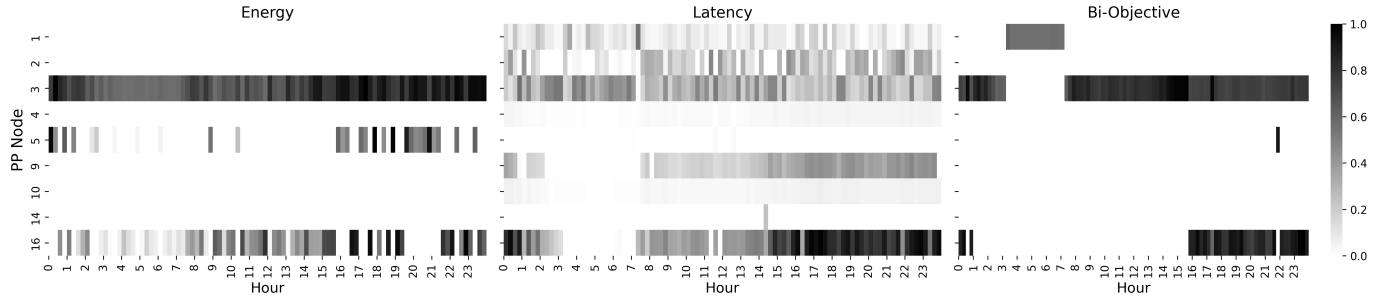


Fig. 10: PP computing utilization for the Mesh Topology

RAN configuration. Two types of topologies are considered, and the MILP is executed under three objective functions: energy minimization, FH latency minimization, and a bi-objective combination.

The results demonstrate that VC selection influences computing utilization, VNF placement, FH and MH latency, and overall energy consumption, while having a limited effect on link utilization. Moreover, the behavior between VC selection and network topology differs across objective functions.

Under energy minimization, RAN functions typically are centralized. In the hierarchical topology, functions are mainly centralized; however, high-demand slices often opt for dual-split VCs to distribute CU and DU workloads across two nodes, guided by distance and PP capacity. In the mesh topology, RAN functions are also centralized and often placed on PPs located near the RUs, increasing the PPs' computing load while leaving RUs lightly utilized. Additionally, some RUs – especially those operating at 20 and 40 MHz – select VC 3 and co-locate the DU and RU to accommodate their relatively lower processing demands. On the other hand, the FH latency minimization results in a different behavior compared to the energy minimization: RAN function placement is more disaggregated. Most of the functions are placed in the cell-site with VC 3, and distributes the DU load into a third node when the demand increases. Finally, the bi-objective results balance energy and FH latency minimization in terms of computing utilization and FH latency, while significantly reducing energy consumption compared to FH latency minimization and remaining nearly identical to energy minimization. In both topologies, the most frequently chosen VC is 3, especially among 20 and 40 MHz RUs. Meanwhile, 100 MHz RUs centralize their VNFs during low-demand periods and distribute them to an independent DU during high-demand periods.

We observed how the network needs to reconfigure to satisfy slice demands while minimizing energy consumption. The bi-objective approach provides a fair balance between energy savings and FH latency reduction. However, the increased complexity of RUs must be carefully considered. Demand levels influence computing loads and thus affect VC selection, as varying channel bandwidth sizes alter both the demand and the necessary computing resources. Notably, the model consistently met latency constraints across all scenarios. These findings underscore the importance of RAN configuration adaptation, allowing dynamic adaptations that maintain performance requirements while optimizing energy utilization.

REFERENCES

- [1] *IEEE Standard for Packet-based Fronthaul Transport Networks*, IEEE Std. IEEE 1914.1-2019, April 2020, published.
- [2] “IEEE standard for local and metropolitan area networks – time-sensitive networking for fronthaul - amendment 1: Enhancements to fronthaul profiles to support new fronthaul interface, synchronization, and syntonization standards,” *IEEE Std 802.1CMde-2020 (Amendment to IEEE Std 802.1CM-2018)*, pp. 1–35, 2020.
- [3] E. Municio, G. Garcia-Aviles, A. Garcia-Saavedra, and X. Costa-Pérez, “O-ran: Analysis of latency-critical interfaces and overview of time sensitive networking solutions,” *IEEE Communications Standards Magazine*, vol. 7, no. 3, pp. 82–89, 2023.
- [4] Rohde & Schwarz, “Network energy saving (nes).” https://www.rohde-schwarz.com/us/solutions/wireless-communications-testing/mobile-network-infrastructure-testing/network-energy-saving-nes_257805.html, 2024, accessed: 2025-06-11. [Online]. Available: https://www.rohde-schwarz.com/us/solutions/wireless-communications-testing/mobile-network-infrastructure-testing/network-energy-saving-nes_257805.html
- [5] A. M. Alba, J. H. G. Velásquez, and W. Kellerer, “An adaptive functional split in 5g networks,” in *IEEE INFOCOM 2019 - IEEE Conference on Computer Communications Workshops (INFOCOM WKSHPS)*, 2019, pp. 410–416.
- [6] A. M.-n. Alba and W. Kellerer, “Dynamic functional split adaptation in next-generation radio access networks,” *IEEE Transactions on Network and Service Management*, pp. 1–1, 2022.

[7] F. Z. Morais, G. M. F. de Almeida, L. Pinto, K. V. Cardoso, L. M. Contreras, R. d. R. Righi, and C. B. Both, "Placeran: Optimal placement of virtualized network functions in beyond 5g radio access networks," *IEEE Transactions on Mobile Computing*, vol. 22, no. 9, pp. 5434–5448, 2023.

[8] G. M. Almeida, V. H. Lopes, A. Klautau, and K. V. Cardoso, "Deep reinforcement learning for joint functional split and network function placement in vran," in *GLOBECOM 2022 - 2022 IEEE Global Communications Conference*, 2022, pp. 1229–1234.

[9] E. Amiri, N. Wang, M. Shojafar, and R. Tafazolli, "Optimizing virtual network function splitting in open-ran environments," in *2022 IEEE 47th Conference on Local Computer Networks (LCN)*, 2022, pp. 422–429.

[10] X. Foukas, N. Nikaein, M. M. Kassem, M. K. Marina, and K. Kontovasilis, "Flexran: A flexible and programmable platform for software-defined radio access networks," ser. CoNEXT '16. New York, NY, USA: Association for Computing Machinery, 2016, p. 427–441. [Online]. Available: <https://doi.org/10.1145/2999572.2999599>

[11] X. Foukas, M. K. Marina, and K. Kontovasilis, "Orion: Ran slicing for a flexible and cost-effective multi-service mobile network architecture," in *Proceedings of the 23rd Annual International Conference on Mobile Computing and Networking*, ser. MobiCom '17. New York, NY, USA: Association for Computing Machinery, 2017, p. 127–140. [Online]. Available: <https://doi.org/10.1145/3117811.3117831>

[12] B. M. Khorsandi, F. Tonini, E. Amato, and C. Raffaelli, "Dedicated path protection for reliable network slice embedding based on functional splitting," in *2019 21st International Conference on Transparent Optical Networks (ICTON)*, 2019, pp. 1–4.

[13] B. Ojaghi, F. Adelantado, E. Kartsakli, A. Antonopoulos, and C. Verikoukis, "Sliced-ran: Joint slicing and functional split in future 5g radio access networks," in *ICC 2019 - 2019 IEEE International Conference on Communications (ICC)*, 2019, pp. 1–6.

[14] B. Ojaghi, F. Adelantado, A. Antonopoulos, and C. Verikoukis, "Slicedran: Service-aware network slicing framework for 5g radio access networks," *IEEE Systems Journal*, vol. 16, no. 2, pp. 2556–2567, 2022.

[15] B. Ojaghi, F. Adelantado, and C. Verikoukis, "So-ran: Dynamic ran slicing via joint functional splitting and mec placement," *IEEE Transactions on Vehicular Technology*, pp. 1–16, 2022.

[16] B. Ojaghi, F. Adelantado, A. Antonopoulos, and C. Verikoukis, "Impact of network densification on joint slicing and functional splitting in 5g," *IEEE Communications Magazine*, vol. 60, no. 7, pp. 30–35, 2022.

[17] W. da Silva Coelho, A. Benhamiche, N. Perrot, and S. Secci, "Function splitting, isolation, and placement trade-offs in network slicing," *IEEE Transactions on Network and Service Management*, vol. 19, no. 2, pp. 1920–1936, 2022.

[18] N. Sen and A. F. A, "Slice aware baseband function placement in 5g ran using functional and traffic split," *IEEE Access*, vol. 11, pp. 35 556–35 566, 2023.

[19] M. Sulaiman, A. Moayyedi, M. A. Salahuddin, R. Boutaba, and A. Saleh, "Multi-agent deep reinforcement learning for slicing and admission control in 5g c-ran," in *NOMS 2022-2022 IEEE/IFIP Network Operations and Management Symposium*, 2022, pp. 1–9.

[20] I. Koutsopoulos, "The impact of baseband functional splits on resource allocation in 5g radio access networks," in *IEEE INFOCOM 2021 - IEEE Conference on Computer Communications*, 2021, pp. 1–10.

[21] T. Pamuklu, M. Erol-Kantarci, and C. Ersoy, "Reinforcement learning based dynamic function splitting in disaggregated green open rans," in *ICC 2021 - IEEE International Conference on Communications*, 2021, pp. 1–6.

[22] F. W. Murti, S. Ali, and M. Latva-aho, "Constrained deep reinforcement based functional split optimization in virtualized rans," *IEEE Transactions on Wireless Communications*, pp. 1–1, 2022.

[23] F. W. Murti, S. Ali, G. Iosifidis, and M. Latva-aho, "Deep reinforcement learning for orchestrating cost-aware reconfigurations of vrans," 2022. [Online]. Available: <https://arxiv.org/abs/2208.05282>

[24] M. Klinkowski, "Latency-aware du/cu placement in convergent packet-based 5g fronthaul transport networks," *Applied Sciences*, vol. 10, no. 21, 2020. [Online]. Available: <https://www.mdpi.com/2076-3417/10/21/7429>

[25] —, "Optimized planning of du/cu placement and flow routing in 5g packet xhaul networks," *IEEE Transactions on Network and Service Management*, pp. 1–1, 2023.

[26] L. M. Moreira Zorello, M. Sodano, S. Troia, and G. Maier, "Power-efficient baseband-function placement in latency-constrained 5g metro access," *IEEE Transactions on Green Communications and Networking*, vol. 6, no. 3, pp. 1683–1696, 2022.

[27] M. S. Akhtar, J. Gupta, M. I. Alam, S. Majhi, and A. Adhya, "Fronthaul latency and capacity constrained cost-effective and energy-efficient 5g c-ran deployment," *Optical Fiber Technology*, vol. 80, p. 103392, 2023. [Online]. Available: <https://www.sciencedirect.com/science/article/pii/S1068520023001724>

[28] H. Gupta, M. Sharma, A. Franklin A., and B. R. Tamra, "Apt-ran: A flexible split-based 5g ran to minimize energy consumption and handovers," *IEEE Transactions on Network and Service Management*, vol. 17, no. 1, pp. 473–487, 2020.

[29] L. M. Moreira Zorello, M. Sodano, S. Troia, and G. Maier, "Power-efficient baseband-function placement in latency-constrained 5g metro access," *IEEE Transactions on Green Communications and Networking*, vol. 6, no. 3, pp. 1683–1696, 2022.

[30] Z. Gao, S. Yan, J. Zhang, B. Han, Y. Wang, Y. Xiao, D. Simeonidou, and Y. Ji, "Deep reinforcement learning-based policy for baseband function placement and routing of ran in 5g and beyond," *Journal of Lightwave Technology*, vol. 40, no. 2, pp. 470–480, 2022.

[31] W. Pires, G. de Almeida, S. Correa, C. Both, L. Pinto, and K. Cardoso, "Bi-objective optimization for energy efficiency and centralization level in virtualized ran," in *ICC 2022 - IEEE International Conference on Communications*, 2022, pp. 1034–1039.

[32] I. Koutsopoulos, "The impact of baseband functional splits on resource allocation in 5g radio access networks," in *IEEE INFOCOM 2021 - IEEE Conference on Computer Communications*, 2021, pp. 1–10.

[33] M. I. Rochman, W. Ye, Z.-L. Zhang, and M. Ghosh, "A comprehensive real-world evaluation of 5g improvements over 4g in low- and mid-bands," 2024. [Online]. Available: <https://arxiv.org/abs/2312.00957>

[34] 3rd Generation Partnership Project, "Technical specification 38.801 v14.0.0: Group radio access network, study on new radio access technology, radio access architecture and interfaces (release 14)," pp. 1–91, 3 2017.

[35] *Technical Specification O-RAN Open Xhaul Transport*, O-RAN ALLIANCE Std. ORAN-WG9.XPSAAS.0-R003-v04.00, 2023, o-RAN Open Xhaul Transport Working Group 9 Xhaul Packet Switched Architectures and Solutions.

[36] S. Lagén, L. Giupponi, A. Hansson, and X. Gelabert, "Modulation compression in next generation ran: Air interface and fronthaul trade-offs," *IEEE Communications Magazine*, vol. 59, no. 1, pp. 89–95, 2021.

[37] J. Wang and Y. Hu, "Architectural and cost implications of the 5g edge nfv systems," in *2019 IEEE 37th International Conference on Computer Design (ICCD)*, 2019, pp. 594–603.

[38] Y. Y. Chun, M. H. Mokhtar, A. A. A. Rahman, and A. K. Samigan, "Performance study of lte experimental testbed using openairinterface," in *2016 18th International Conference on Advanced Communication Technology (ICACT)*, 2016, pp. 617–622.

[39] B. Debaillie, C. Dessel, and F. Louagie, "A flexible and future-proof power model for cellular base stations," in *2015 IEEE 81st Vehicular Technology Conference (VTC Spring)*, 2015, pp. 1–7.

[40] C. Dessel, B. Debaillie, V. Giannini, A. Fehske, G. Auer, H. Holtkamp, W. Wajda, D. Sabella, F. Richter, M. J. Gonzalez, H. Klessig, I. Góðor, M. Olsson, M. A. Imran, A. Ambrosy, and O. Blume, "Flexible power modeling of lte base stations," in *2012 IEEE Wireless Communications and Networking Conference (WCNC)*, 2012, pp. 2858–2862.

[41] "Common public radio interface: Requirements for the cpri transport network, version 1.2," <http://www.cpri.info>, Ericsson AB, Huawei Technologies Co. Ltd, NEC Corporation, and Nokia, May 2019, interface Specification. Common Public Radio Interface: eCPRI Interface Specification. Developed by Ericsson AB, Huawei Technologies Co. Ltd, NEC Corporation, and Nokia.

[42] D. Kliazovich, P. Bouvry, Y. Audzevich, and S. U. Khan, "Greencloud: A packet-level simulator of energy-aware cloud computing data centers," in *2010 IEEE Global Telecommunications Conference GLOBECOM 2010*, 2010, pp. 1–5.

[43] CTTC, SMO, TID, and TUE, "D 2.2 overall network architecture and control aspects definition," Project PASSION, Research and Innovation Action – RIA Grant number 780326, January 2020, project title: Photonics technologies for ProgrAmmable transmission and switching modular systems based on Scalable Spectrum/space aggregation for future agile high capacity metrO Networks. [Online]. Available: <https://ec.europa.eu/info/funding-tenders/opportunities/portal/screen/opportunities/topic-details/h2020-ict-30-2017>

[44] Intel Corporation, "APP Metrics for Intel® Microprocessors - Intel® Xeon® Processor," <https://www.intel.com/content/www/us/en/content-details/840270/app-metrics-for-intel-microprocessors-intel-xeon-processor.html>, 2024, content ID: 840270, Published: 2024-01-04. [Online]. Available: <https://www.intel.com/content/www/us/en/content-details/840270/app-metrics-for-intel-microprocessors-intel-xeon-processor.html>

[45] SPEC, “All published specpower_ssj2008 results,” 2024, last update: Wednesday, 10 July 2024, 14:24. Published Results (1018). These results have been submitted to SPEC; see the disclaimer before studying any results. [Online]. Available: http://www.spec.org/power_ssj2008/results/power_ssj2008.html

[46] Cisco Systems, Inc., *Cisco ASR 9000 Series Aggregation Services Router Overview and Reference Guide*, Cisco Systems, accessed: 2025-04-03. [Online]. Available: https://www.cisco.com/c/en/us/td/docs/iosxr/asr9000/hardware-install/overview-reference/b-asr9k-overview-reference-guide/b-asr9k-hardware-installation-guide_chapter_011.html

[47] 3GPP, “5g; nr; physical channels and modulation (3gpp ts 38.211 version 16.2.0 release 16),” 3rd Generation Partnership Project (3GPP), Technical Specification 3GPP TS 38.211 version 16.2.0 Release 16, 2020.

[48] P. D. Francesco, F. Malandrino, and L. A. DaSilva, “Assembling and using a cellular dataset for mobile network analysis and planning,” *IEEE Transactions on Big Data*, vol. 4, no. 4, pp. 614–620, 2018.

[49] A. Checko, H. L. Christiansen, Y. Yan, L. Scolari, G. Kardaras, M. S. Berger, and L. Dittmann, “Cloud ran for mobile networks—a technology overview,” *IEEE Communications Surveys & Tutorials*, vol. 17, no. 1, pp. 405–426, 2015.